CHAPTER 4

SOME APPLICATIONS USING DENSE CORRESPONDENCE PROPERTIES

4.1 Introduction

In the previous chapter, a method to reparameterize shapes into corresponding meshes was presented. The output meshes of a class of shapes are such that they are all described by the same number of vertices, and each vertex is on the same anatomical location for all instances of the class. The method was applied on a database of wrist bones, the output meshes are called $M_{W,\{b,i\}}$, b characterizing the class of bone the shape belongs to, i is the index of the person in the database.

In this chapter, we propose various applications of such a database, composed of corresponding bones. The first application is the computation of statistical shape models. They consist in a statistical analysis of the location or deformation of the mesh vertices over the instances, and can only be computed when the shapes are in correspondence. Most of the time, the modeling is based on a Principal Component Analysis of the forms, or derivative methods. We compute such a model, both as a reference and because the correspondence quality factors proposed in [DCT01] rest on a SSM computation. In a second time we compute a Gaussian process based model. The latter is less common and has never been used on wrist bones, but offers numerous advantages over SSMs, such as non-linearity and adaptation to posterior information. We carefully test the models in order to verify their reliability.

In a second phase, we use the SSMs to register a second wrist database. It offers two advantages: the model can be further tested on new data and the modeling of this other database with the SSMs is naturally in correspondence with the bones of the training database. We prove that the resulting shapes are very similar to the original ones. The method presented in Chap **??** is not used on this database because the final purpose of the work is to create accurate tools for real-life applications, and evaluation of the model on unknown data is more interesting. Furthermore the data of this second database are less complete than the one used in the previous chapter, the metacarpals are only partially visible, the radii distal end are shorter. Using complete models on these data bring information about the unavailable parts of the bones.

Finally, we propose a third application for the corresponding meshes. We prove that the properties of these meshes allow the definition of any system of coordinates on example instances. The latter can be reproduced on all other occurrences of the database. Such systems are employed in biomechanics, the study of a joint movement is based on the rigid transformations of one system relatively to the other. We prove that the method is as reliable as another specific one proposed in the literature while being more global. The results additionally strengthen the confidence in the correspondence relations quality between the meshes, as the method is entirely based on the correspondence features.

4.2 Statistical Shape Model

In a first time, we propose to use the correspondence relation between the database meshes to construct statistical shape models. These latter are a common application for meshes in correspondence. They enable the analysis of shapes distribution by describing the main variations among a class. They can be used for various operations: for example the characterization of the main shape variations among a population allows a better understanding of the shapes studied. The statistical models are also often used as prior knowledge for image segmentation, which allows more stable and precise results. They can also be used for development of subject-specific prosthesis, or else 3D information can be retrieved from 2D images using the additional knowledge of the model.

In this thesis, the models are used for none of the previously cited applications. We endeavor to create statistical models that should be convenient and reliable and measure their limits. They can afterwards be used for any aforementioned application, once their expected precision is established. We especially propose to work with Gaussian Process Morphable Models (GPMMs), an extension of PCA-based SSMs, that have been little used by now. In particular, to the best of our knowledge, they have never been used for wrist bones encoding. The additional computation of PCA-based SSMs have two purposes: it enables comparison with GPMMs and it is required for the computation of correspondence quality criteria.

The section starts with a brief state-of-the-art of existing statistical shape models. Then PCA-based SSMs are computed and analyzed, both models describing individual bones and a model characterizing the whole wrist at once. Then a more complex statistical model is used, based on Gaussian Processes, and the practicality of such a model for our data is discussed.

4.2.1 State of the art

With computers come the will and need to automate as many tasks as possible, with the most accurate outcomes achievable. One of the great goals of computer scientists has been since quite early the automation of image interpretation. One key step to achieve it is the ability to recognize and delineate objects in pictures. Yet in a same class of objects, shapes change over instances, and sometimes instances themselves transform over time. It is especially the case in medical imaging, every patient's organs are uniquely shaped, and they evolve over time, whether fast, such as beating hearts or more slowly. The need to adapt an initial object to the shape of the considered instance has risen.

Different solutions were proposed over time to segment variously shaped instances of the same class of objects. Model-based segmentation is a top-down approach consisting in matching a model containing information about the class expected shape with new images. It it one of the most successful existing methods, the prior information brought by the model provides stability against image artifacts and perturbations [HM09]. The flexibility of the model enables adaptation to the various instances of the class. We focus on this segmentation approach.

One of the first flexible model was introduced by Kass et al. [KWT88] and is called Active Contour Models or Snakes. In consists in describing the contour of an object as a continuous spline subjected to forces controlling compliance to image features and fulfillment of structural constraints such as smoothness. However, snakes lack specificity as they don't incorporate knowledge about shape variations in the class and are not restrained in their distortions as long as the energies are minimized [DTT08].

Information about common variations need to be added in the model. One straightforward approach consists in considering multiple instances of the object class as training shapes and learning from the set statistical properties of the class [HM09]. It leads to Statistical Shape Models (SSMs), most of them being based on a Principal Component Analysis (PCA), which is further detailed in Sec. 4.2.2. The first SSM was introduced by Cootes et al. in [CHTH94] and was more detailed later in [CTCG95]. The statistical analysis of the training set is computed using PCA: they work with shapes described by landmarks, and analyze the points positions distribution over instances. This distribution is called Point Distribution Model (PDM). The model based on the PDM used for image segmentation is named Active Shape Model. Another popular SSM was introduced by Blanz and Vetter, called the Morphable Model. It is used for generation of new human faces and extraction of a 3D mask from a 2D picture, also based on PCA [BV+99].

PCA-based models are linear, which makes them mathematically easy and fast to compute. They can only represent linear combinations of the training shapes, which makes them robust towards artifacts and noise [LGJV17]. However this limitation to the linear span defined by the training set is both an advantage and a downside of the method. It prevents the apparition of impossible shapes, but it also stops the model from generating accurate shapes too different from the training set. To overcome this problem, the training data should be as numerous and various as possible.

For PCA-based models, the training set should ideally be very large, however this is often not possible, in particular when working with medical images. Therefore, works have been conducted to reduce the impact of limited quantity of data for the model creation. Artificial training data can be used, as in [CT95]. Cootes et al propose to add artificial training data using finite element models (FEM). These latter give a set of linear deformations of one shape corresponding to its modes of vibration. They generate many new shapes using FEM on every instance of the training set, and use all original and generated shapes to train the SSM. However, the variations of the FEMs are arbitrary and may not be representatives of the real variations of the class of shapes. In order to extend the flexibility of the model, a spatial partition of the object can also be a solution, as proposed by Zhao et al in [ZAT05]. They partition shapes in tiles, and apply a PCA to each tile separately, before projecting the results in one hyperspace to ensure coherence between the fragments. Blanz and Vetter [BV+99] propose a similar partitioning of the total shape in sub-regions, which were morphed individually before being blended back together. Finally, another solution consists in decomposing the shapes in the frequency domain as proposed by Davatzikos et al [DTS03], and later improved by Nain et al. [NHBT07]. The hierarchical multi-scale formulation of SSMs is based on a wavelet transform of the points positions.

Wang and Staib chose to improve the SSM by working on the covariance matrix, rather than on the data [WS00]. They introduce the covariance matrix based on the PDM of the training data, but they also propose a covariance matrix describing smoothness constraint between neighboring points. Finally they combine both matrices to associate the specificity brought by the model trained on the data with the variability of the smoothness constraint. Lüthi et al propose in a series of articles summarized in [LGJV17] a similar idea of SSM but extended. Their model is based on Gaussian Processes and is further detailed in Sec. 4.2.3. They call it Gaussian Process Morphable (GPMM) Model. The GPMM can be viewed as an extension of the PCA-based SSM, in that it is more complete. Gaussian Processes were already used in the 90's for image registration, as referred in the overview by Grenander et al. [GM98]. Lüthi et al. argue that in their version using the Nyström approximation any combination of kernels can be used, which makes the method so powerful.

In this state of the art, we have focused on models for shapes characterized by landmarks distributed over the object, and already in dense correspondence. It is indeed the type of data we're working with (cf chapter **??**). However, different shape characterizations, such as skeletons representations, surface encoding with Spherical Harmonics or Fourier surfaces lead to diverse models.

In the following sections, two statistical models have been implemented: a PCA-based Statistical Shape Model and a model based on Gaussian processes. The theory behind the models, as well as the results achieved are presented and discussed.

4.2.2 Principal Component Analysis

The Principal Component Analysis, also called PCA, is a statistical procedure used to extract the principal modes of variations of data. It can also be used for dimensionality reduction of data, as will be further explained. It has been widely used for image segmentation, the PCA being used as prior information about the object class shape in the form of a Statistical Shape Model. It can have other applications, such as shape analysis by examination of the main modes of variations or investigation of the impact of some factors such as gender. Finally, as previously mentioned in Chapter **??**, the SSM is a mean of measuring correspondence quality.

We chose to apply PCA on our data. It is aimed at controlling the quality of the correspondence results previously computed. It is also meant for comparison with the Gaussian Process Morphable Model later computed. First we detail the PCA procedure (further details can be found in Jolliffe's work, for instance in [Jol11]). Then we explain and examine our results.

The procedure requires multiple properties of the data: the data must follow a Gaussian distribution. In the case of coordinates of landmarks, the shapes must be previously similarly aligned, oriented and scaled, to avoid noise. We make the assumption that the bone shapes indeed follow a Gaussian distribution, which is a classical hypothesis. As explained in Chapter **??**, all bones were previously aligned and scaled using ICP, this condition is met.

4.2.2.a What is the Principal Component Analysis?

The Principal Component Analysis is a statistical procedure that evaluates the distribution of a set of data, and transforms them to a new space of uncorrelated components, which often leads to a dimensionality reduction.

Let's suppose we have n measurements of a vector $\mathbf{x}$ of p random variables. These variables are potentially correlated. PCA transforms the data to a new space of uncorrelated variables. The axes of this new space are a set of orthogonal vectors, the origin of the coordinate system is the projection of the mean shape $\bar{\mathbf{x}}$ in the new space. PCA determines a set of orthogonal axes, which maximizes the variance along each axes. These axes are determined in such a way that they successively have maximum variance for the data, while being uncorrelated with previously computed axes. The number of distinct non-zero vectors is $q = \min(n-1, p)$, which often leads to a reduction of dimensionality. An example of principal components can be seen in Fig. 4.1.

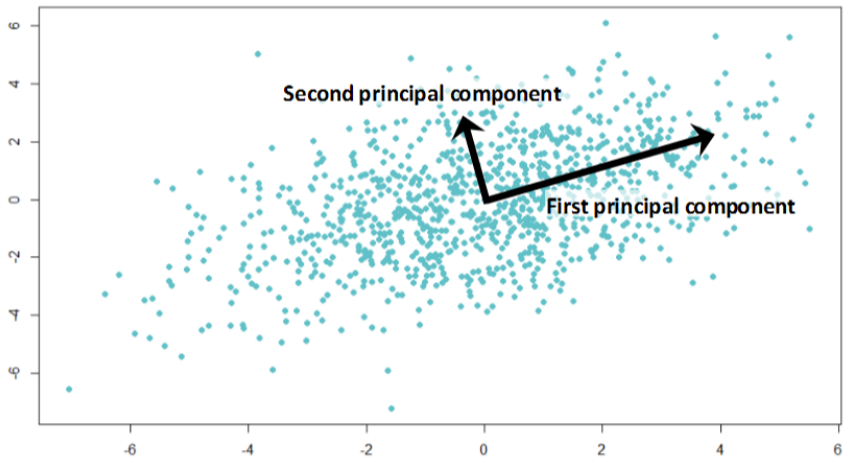

Figure 4.1: Example of a Principal Component Analysis. The first component is the axis on which there is the most variability when the data are projected on to it. The second axis is perpendicular to the first one. The center of the new system is the center of mass of the data. Illustration from *medium.com*

It can be proven that the orthonormal directions that maximize the variance associated to each vector are given by the eigenvectors of the data covariance matrix, corresponding to the q largest eigenvalues [DTT08]. The eigenvalues give the variances associated to each eigenvector, the latter are ordered from the highest eigenvalue to the smallest one. To avoid the domination of a few high-variance variables over the others or in the case of different units, the variables are often standardized to have zero mean and unit variance [Jol11].

The PCA is computed as follows. At first the mean shape is calculated, as a simple average over the n measurements.

$$\bar{\mathbf{x}} = \frac{1}{n}\sum_{i=1}^{n}\mathbf{x_i} \tag{4.1}$$

Let $\mathbf{X}$ be the matrix $(n \times p)$ composed of all measurements of vector $\mathbf{x}$, and $\mathbf{X_c}$ the standardized matrix such that:

$$\mathbf{X_c}(i,j) = \frac{\mathbf{X}(i,j) - \bar{\mathbf{x}}(j)}{\sigma(\mathbf{X}(:,j))} \tag{4.2}$$

$\sigma(\mathbf{X}(:,j))$ is the standard deviation of the j^{th} variable of all measurements of $\mathbf{x}$. The covariance matrix C is computed, using standardized values.

$$C = \frac{1}{n-1}\mathbf{X_c}^t\mathbf{X_c} \tag{4.3}$$

Then, the eigenvectors matrix V and their associated eigenvalues Λ are defined such as:

$$CV = \Lambda V \tag{4.4}$$

Only the q non-zero eigenvalues and their associated eigenvectors are considered. The matrix V maps the data from the original space towards the new space, while V^t allows a mapping from the new space back to the original space. A measurement of $\mathbf{x}$ expressed in the new base, called x_n, is equal to:

$$x_n = (\mathbf{x} - \bar{\mathbf{x}})V\sqrt{\Lambda^{-1}} \tag{4.5}$$

New measurements of $\mathbf{x}$ can be simulated by generating random vectors w of size q, with each value $w_i \sim \mathcal{N}(0,1)$. Usually the values are forced to take their value in the interval $[-3;3]$. [1] The vector of size q is the representation of the simulated measurement in the new space. In the original space, the simulated measurement is equal to:

$$\mathbf{x_w} = \bar{\mathbf{x}} + wV^t\sqrt{\Lambda} \tag{4.6}$$

It should be noted that the mapping are not exactly the inverse transformations of each other, even if all non-zero eigenvectors are retained, since the dimensionality

[1] Let X be a random variable, with a normal distribution of mean μ and standard deviation σ. Let x be a value taken by X. Then $P(x \in [\mu - 3\sigma; \mu + 3\sigma]) \geq 99.7\%$. Which means that almost all values that can be taken by X will be in the interval $[\mu - 3\sigma; \mu + 3\sigma]$ with a very small chance of error.

We make the assumption that the distribution of $\mathbf{x}$ is a multidimensional normal distribution. The eigenvalues associated to the eigenvectors represent the variance of the modes. The square root of an eigenvalue gives the standard deviations of the mode sd. Then with a similar reasoning than in one dimension, with a very small error, we can define the range of all possible shapes as all those that can be described as a summation of the mean vector and the weighted eigenvectors, each weight w_i being such as $w_i \in [-3; +3]$

of parameter space is less than the dimensionality of shape space [DTT08]. If a new observation of $\mathbf{x}$ is projected into the new space, then transformed back into the original space, it will not be strictly identical to the initial observation. Indeed the first transformation is a projection into the subspace defined by the training set, then it is transformed back through a linear interpolation of the training set measurements, using the available modes.

Most often the last eigenvectors are associated with small variance, information added by these vectors is poor. When there are not many data, it can even be strongly linked to one of the measurement, and falsely add variance to the model, which can worsen the results. Therefore, the last eigenvectors are often ignored, and only the largest ones are considered. The number of vectors kept can be chosen according to multiple criteria: the cumulative variance should be higher than a defined proportion of the total shape variance, for instance 95% or 99%. Or else the number of vectors kept should enable to reach a certain precision of data when using the model. In this case, the number q of considered vectors is smaller than the number of non-zeros eigenvalues. The equations are still true, V and Λ are simply replaced by their truncated versions.

The registration of a SSM to a target shape consists in minimizing the distance between the target mesh x_{target} and the deformed model $\mathbf{x_w}$. The optimization is computed over the vector w, which describes the weight associated to each mode. We use the mean distance d_{mean} defined in (**??**) as the reference distance between meshes to be reduced.

A statistical model of 3D shapes is constructed by using the position of the meshes vertices. A mesh is described by p vertices in the 3D space. All coordinates are appended in a vector of size $3p$. The shapes are gathered in a matrix of size $(n \times 3p)$, with n the number of available shapes. This matrix of data $\mathbf{X}$ is the one used for the PCA computation. The model describes the vertices location, a shape is recreated from the positions using the same edges and faces as in the training set. In the following section, such a model has been computed on our data, the results are presented.

4.2.2.b Application and validation

As a result of the processes applied in Chapter **??**, our bones are described by 3D meshes that have been aligned, rotated and scaled in such a way that only shape differences are the cause of variations among the bones. The meshes are in dense correspondence and we make the assumption that the distribution of the bone shapes is a multidimensional normal distribution. All conditions necessary for PCA computation are met, we present a statistical model of our data.

Models computation

We chose to calculate two different types of PCA: one per bone and one for the whole wrist including the 14 bones. Both models are interesting as they bring various information. A model for one bone includes less information, and can therefore be more specific and will better capture the details of the bones. Registration results will be more precise. However, if the model of the whole wrist will be less detailed, it has the benefit

of considering neighboring bones altogether. The carpal bones are small and really close to each other, the shape of one necessarily influences its neighbors, the complete model takes it into account. It enables the study of how bones affect each other. This hasn't been studied yet, to the best of our knowledge.

The two main modes of variation of the whole wrist model are shown in Fig. 4.2. The most important variation of shape for the wrist bones is the length and thickness of the metacarpals. In the database they evolve between long and thin to shorter and thicker. It can be noted that quite logically the five of them evolve in the same way, they are all either long or short. The second most important mode of shape variation in the wrist is more subtle to observe on the illustration of Fig. 4.2. The radius styloid form evolves, being either further forward or backward. In the same time the extremities of the metacarpals change from being flatter and in the continuity of the bone to being more brought out. The lunate for its part present a concavity or not. The analysis of the modes of variation is interesting for a better understanding of the different types of wrists existing, and for later classification of new wrists for instance.

When a SSM is computed, one of the parametrization decision to make is the number of vectors that should be used. When the number of data is small, the vectors associated with small variance are sometimes too specific and should be associated rather with noise than with valuable information. To determine the number of vectors that should be used, the models were used to approximate new shapes. The evolution of the registration precision compared to the number of modes used was analyzed. The new shapes outside the training set needed for such an application were obtained with a leave-one-out method: every patient of the database was by turn left out of the training shapes and the model was registered to it. Both individual models and the whole wrist one number of modes were investigated this way.

Registration of the models to the patients

The maximum number of modes available for a model is the minimum value between the number of measurements minus one and the dimensionality of one measurement. In our case the number of patients is the limiting factor, 43 of them were complete wrists, making 41 the maximum number of non-zero vectors for the models when a subject is left out of the training set. Therefore the models were by turn registered to the target patient using $5, 10, 15, 20, 25, 30, 35, 37, 38, 39, 40, 41$ modes. The evolution of the distance between the target mesh and the registered models were computed, using both mean distance (**??**) and Hausdorff distance (**??**) between meshes. The results of the individual models are shown in Fig. 4.3 for the mean distance, in Fig. 4.4 for the Hausdorff distance. The results of the complete model are similarly shown in Fig. 4.5 for the mean distance and in Fig. 4.6 for the Hausdorff distance. It must be noted that if all bones are considered at once in the model, the distances are nonetheless measured for every bone separately.

Considering the individual models, one per bone, it can be noted that the registration gets strictly better when the number of modes used gets higher. No level is reached, where additional modes are unhelpful due to noisy information. This is true for all bones and both mean and maximal distances. The curves presented in Fig. 4.3 and

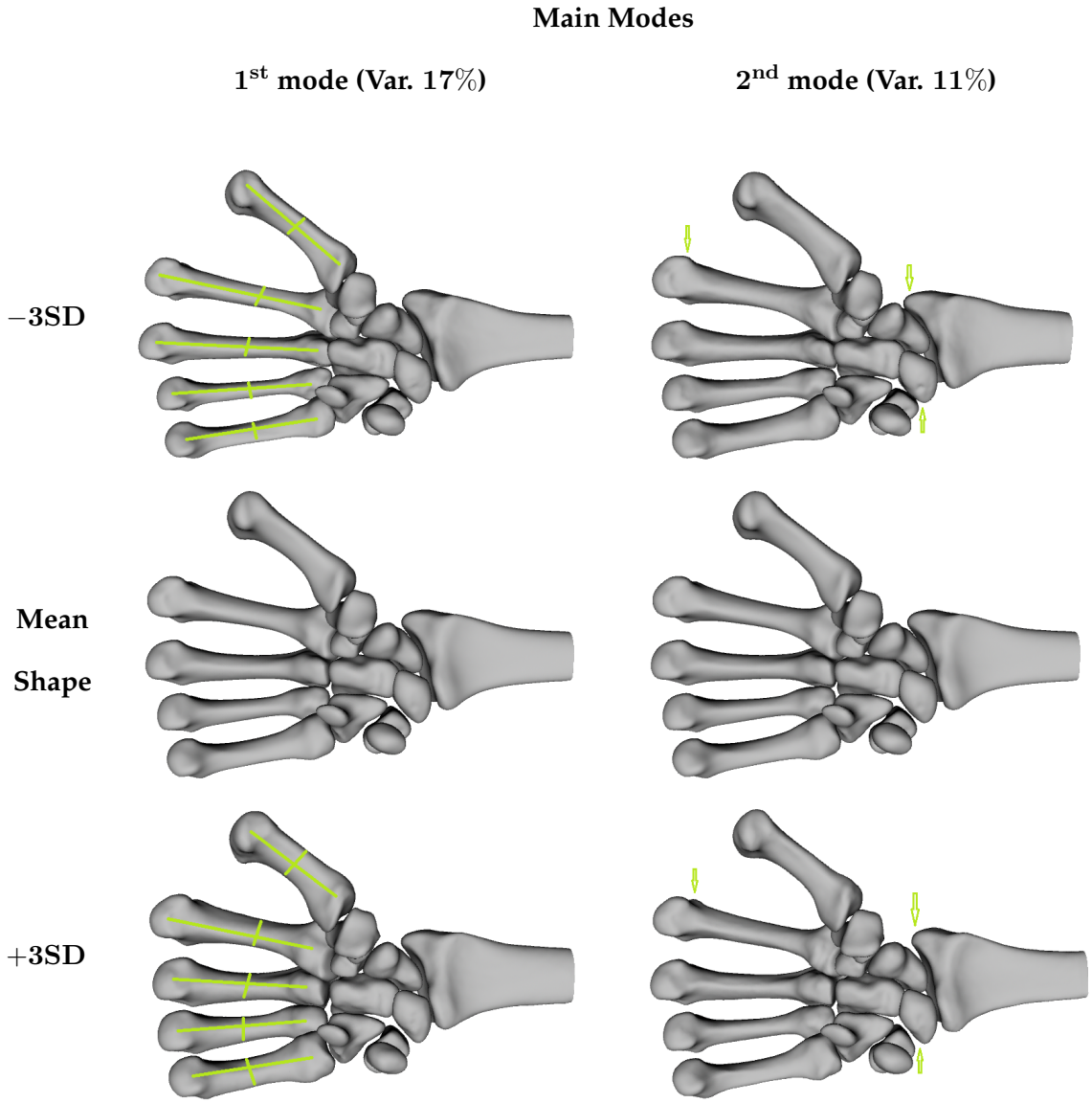

Figure 4.2: The two principal modes of variation of the SSM including the 14 wrist bones. In the middle is shown the mean shape of the wrist bones, while above and under are illustrated the effects of the two principal modes of variation, at extreme values. In the left column is shown the most important mode, in the right the second most important ones. The two modes are associated with respective variances of 17% and 11% of the total model variance.

Fig. 4.4 are strictly decreasing. We can note that the mean distance between the target mesh and the registered model is strictly smaller than 0.3 mm for all bones when enough vectors are considered in the model. The mean error committed between a vertex and its closest point on the paired surface is smaller than the precision of the initial data ($0.33 \times 0.33 \times 0.625$ mm). The Hausdorff distance between the target and the model lies between 0.7 mm and 1.6 mm. The smallest difference is for the pisiform, which is the smallest carpal bones, with both the less complex shape of all and the smallest number of points to represent it (see Table **??**), enabling more details to be captured by the model. The highest difference is between the radius model and its target. This is due to the fact that it is the biggest bone, with the most vertices. Moreover the opened end of the radial styloid is an additional difficulty, that in spite of being taken into account in the distance measurement, has nonetheless a bad impact on the results.

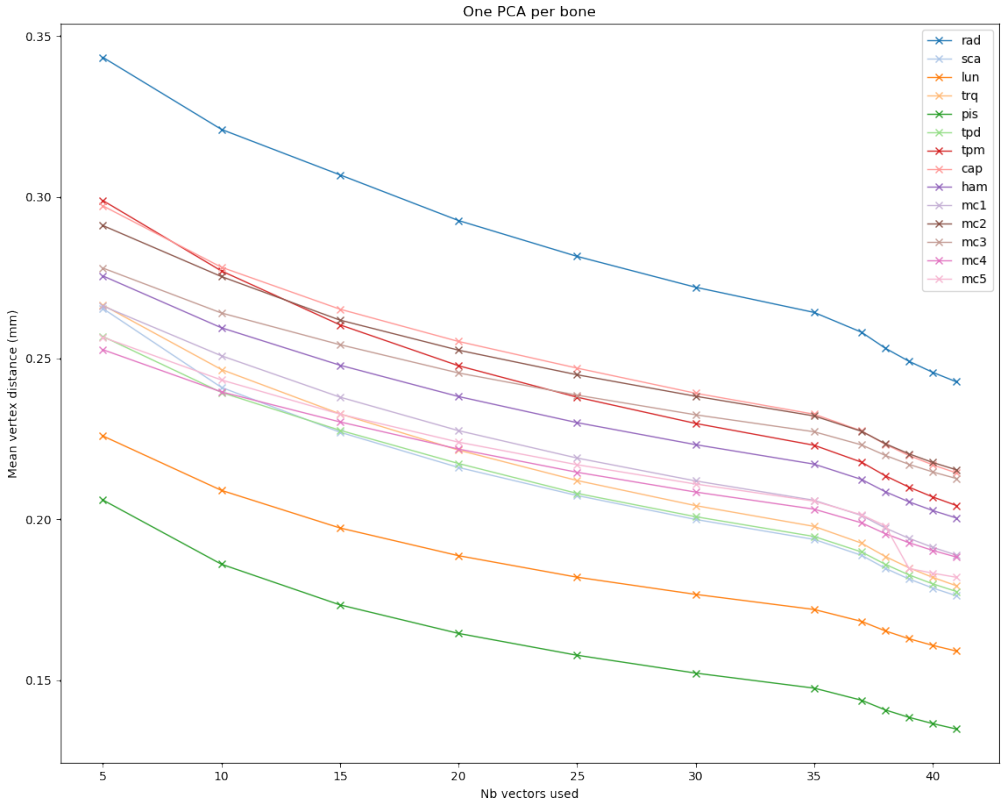

Figure 4.3: The influence of the number of principal modes used for the SSM registration. Each bone is captured by its individual model, every patient is by turn left out of the training set before being targeted by the models. The distance is computed between the registered model and the target meshes using a mean distance (**??**).

When considering the model of the whole wrist, the results are more complex. While the distances for most of the bones between the model and the target meshes decrease with the number of modes used, for some bones they increase instead. Finally for some of them, the distance starts by increasing with the number of modes, before decreasing. It can also be observed that the curves between the mean and the Hausdorff distance in

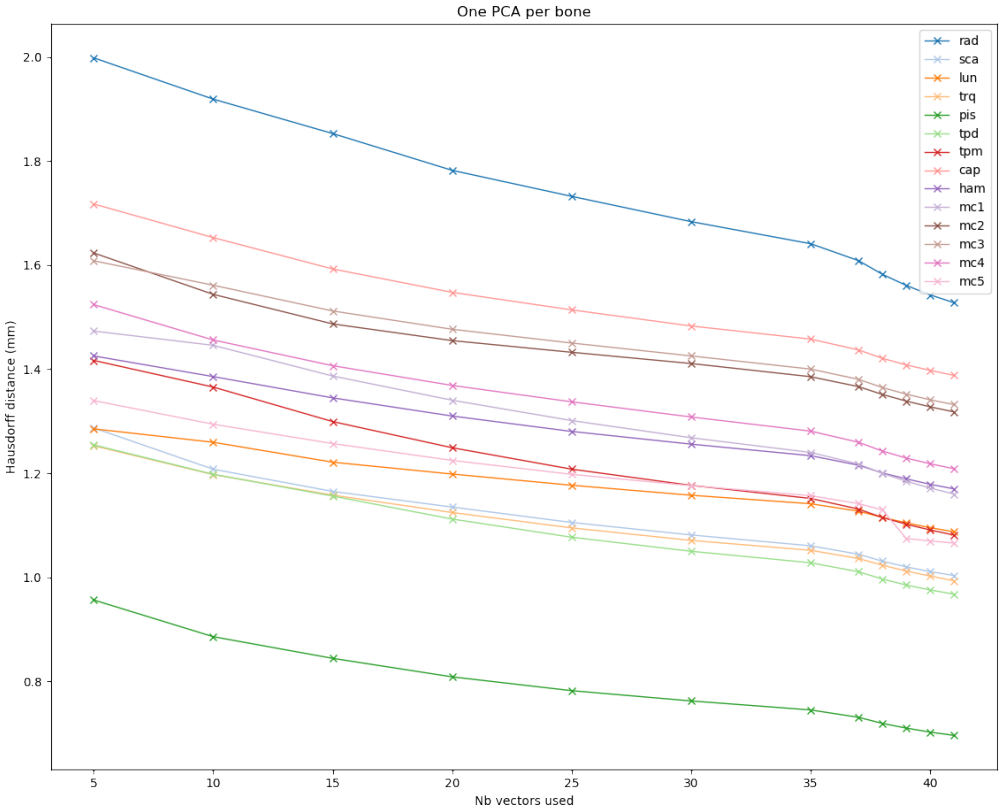

Figure 4.4: The influence of the number of principal modes used for the SSM registration. Each bone is captured by its individual model, every patient is by turn left out of the training set before being targeted by the models. The distance is computed between the registered model and the target meshes using the Hausdorff distance (**??**).

Fig. 4.5 and Fig. 4.6 are not similar while they look a lot alike when individual models are considered.

The bones with the most vertices, such as the radius and the metacarpals become strictly closer to the target shapes in mean distance when the number of modes increases. This is due to a stronger influence on the mean value compared to bones with less vertices. On the opposite, it can be noted that the pisiform, the bone with the less vertices has a distance strictly increasing with the number of modes used. For 8 bones out of 14, the mean distance between a vertex and its closest point on the paired surface is smaller than 0.32 mm, which is also smaller than the precision of the original data. However for the rest of them, the mean distance is higher than 0.33 mm. The Hausdorff distance is included in [1.1; 2.0] mm.

The mean distance when individual models are used is below the acquisition precision. However the maximal distances are still high, some details are present in one person only of the database. When the latter is taken off the training set and the models are registered to its bones, these details are not captured by the model, as testified by the high maximal distances. We can conclude that a larger training set would give better results, although these are already satisfying. Concerning the SSM modeling all wrist

bones at once, the gap between the target bones and the model is too large. The number of data available are not enough for such a complex model, details are buried in the general shapes of the bones. It must also be noted that various profiles of people have been scanned to compose the CMC database. Young and old people, males and females. However nothing guarantees that all types of wrists are present in the database, and these results rest upon the quality and diversity of the database.

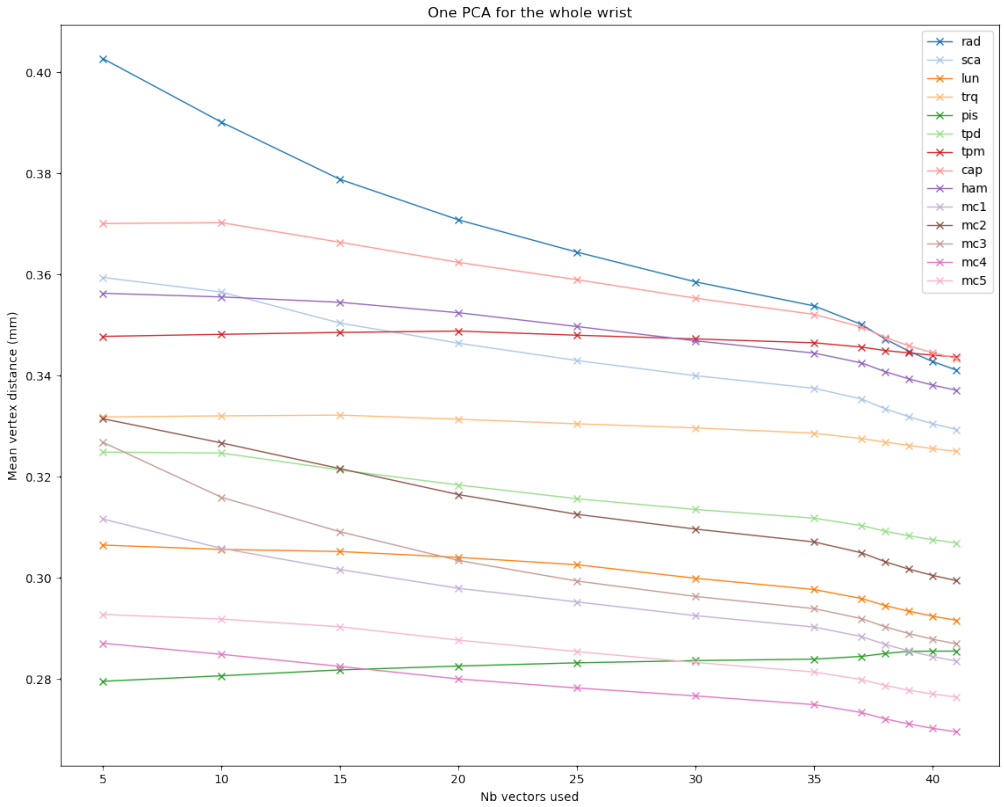

Figure 4.5: The influence of the number of principal modes used for the SSM registration. The whole wrist is captured by the model, every patient is by turn left out of the training set before being targeted by the model. The distance is computed between the registered model and the target meshes using a mean distance (**??**), the distance to each bone being separately measured, while all bones were deformed at once by a unique model.

Correspondence quality factors

In a second time, we use the individual SSMs of the bones to evaluate the correspondence quality factors between the meshes $M_{W\{b,i\}}$ previously generated. Indeed we have so far only been concerned by shapes similarity (Sec. **??**), not correspondence between vertices.

The evaluation of the correspondence relations proposed by Davies et al. [DCT01] (Sec. **??**) is based on the quality of the SSMs resulting from the corresponding meshes. We present the values for the 3 factors: compactness, specificity and generalization in Table **??**. The factors definitions were presented in Sec. **??**. For all factors, the lower the

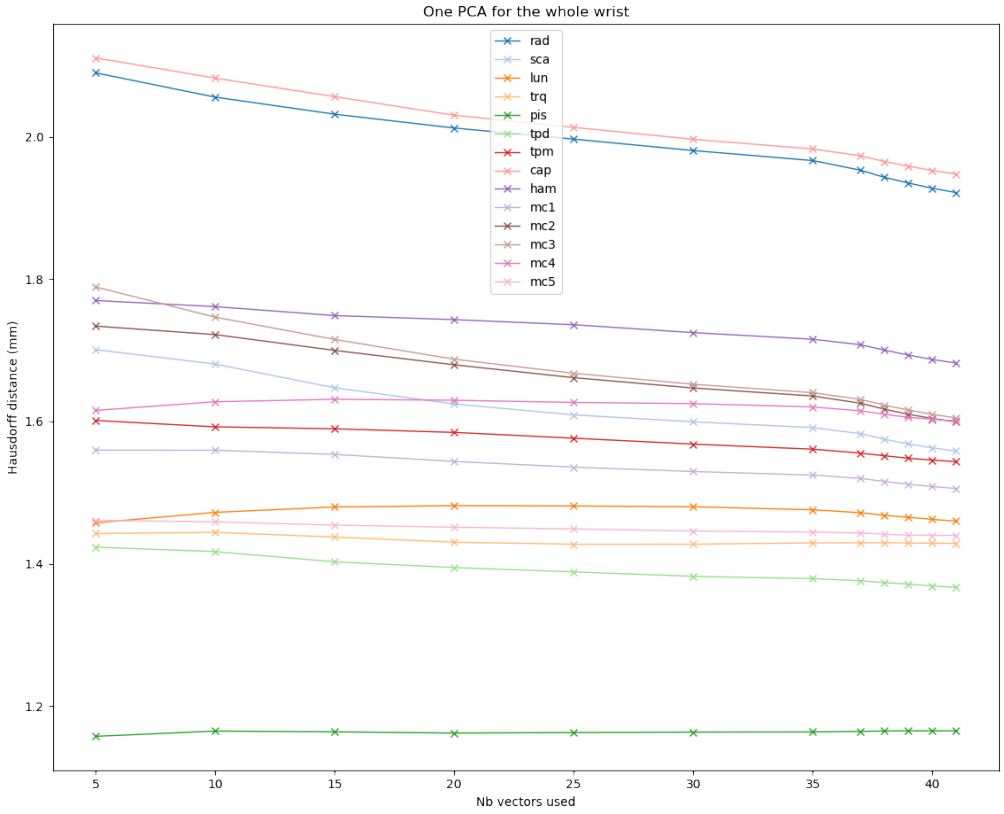

Figure 4.6: The influence of the number of principal modes used for the SSM registration. The whole wrist is captured by the model, every patient is by turn left out of the training set before being targeted by the model. The distance is computed between the registered model and the target meshes using the Hausdorff distance (**??**), the distance to each bone being separately measured, while all bones were deformed at once by a unique model.

value is, the better. However, specificity and generalization of a model are opposite goals, one can only be improved at the expense of the other.

We have computed these factors based on 39 principal modes for each individual model, one model describing one bone. The three factors are useful to compare various correspondence methods used on a same database. However, they can not be interpreted on their own. We give their values in Sec. **??** as reference, should anyone propose another set of corresponding meshes from the same database.

PCA-models are frequently used for the modeling of 3D shapes. They are easy to compute and to employ. Such SSMs are convenient for encoding prior information about classes of shapes. However, they are linear model, and if they are robust towards noise, they can only represent shapes that are in the linear span of their training set. We propose therefore in a second phase to work with statistical models based on Gaussian processes, which can describe a larger span of shapes from the same training set by enforcing other properties of the shapes deformations, such as smoothness.

4.2.3 Gaussian Processes

Models based on a principal component analysis are commonly used for shape analysis and prior information for image segmentation for instance. We propose to use models based on Gaussian processes. It rests on two observations: PCA-based models are linear, and can only represent shapes in the span of their training set. Non-linear models could widen the range of shapes that can be represented, which is especially interesting when the quantity of data available is small. Moreover the use of PCA-based models are entirely automatic, users have no possibility of intervention, even when it is clear to a human eye that the model misses something. It is all the more regrettable that professionals accumulate a lot of knowledge that cannot be used. Gaussian processes can be used to create parametric models that are non-linear. They can also integrate knowledge provided by a user in their prior information and adapt consequently the model. We will firstly detail the reasons that make Gaussian processes so appealing for modeling. Then we will briefly introduce the mathematical background (for further details, the reader is referred to [LGJV17, Duv14, WS01]). Finally, we will present the two models that we have computed: a parametric one, entirely automatic and another one intended for user interaction.

Statistical models based on a Principal Component Analysis are linear parametric models. They are very specific, due to their limited capacity of representing shapes that are necessarily in a linear span of the training set. This specificity is an upside, it makes the model robust towards artifacts and noise. However, this specificity can also be a downside when the training set is small, it jeopardizes the generalization capacity of the model [LFGV17]. Yet appropriate databases can happen to be small, in particular for medical images. Furthermore, if the training data are composed of healthy subjects only, the model will be unable to characterize damaged instances of the class. It may be enough for automatic detection of irregularities, but the model won't be able to adapt to the new instance. Finally these models are by nature designed to be embedded into all-automatic algorithms. The user has no control over the results.

Gaussian process models characterize the possible deformations of a shape based on kernels. The kernels can describe prior information based on training data, but can also be analytically created to enforce properties such as smoothness or symmetry. Multiple kernels can be combined to blend their features. The use of such customized kernels enables the non-linearity of the model, and the span of the possible shapes represented by the model is widen compared to the PCA-based model. It allows to reduce the bias induced by a limited number of instances in the training set. A second property of such a model is that depending on the kernel used, if the latter is independent of any training set, the model can describe a continuous shape independently of the points distribution. The model is also able to integrate new posterior information, and to adapt to take it into account. It enables user interaction, a human can indicate the location of some points. It can especially be handy for degenerated shapes that can not be grasped by the model based on its kernel only. Additional human information for wrong points would enable the characterization of any form. Theoretically, helped with external knowledge, any precision of registration could be reached. The final results can be validated by the user, which enable the use of external knowledge brought by specialists having years of experience.

Even if the Gaussian Processes are widely used in different domains, the application to statistical shape models are not very widespread yet, and to our knowledge, have never been used for bone wrist shapes. Indeed all existing statistical shape models of wrists are based on a Principal Components Analysis (PCA), or derivative methods. We propose to use a model for two applications: one fully-automatic registration of shapes, to compare with the PCA-based model, and another one fully dependent on external information: the expected corresponding final set-up is a continual interaction between the algorithm and the user, who gives any information he judges needed.

Our work has been mostly based on Lüthi et al articles [LJV13, LFGV17, LGJV17].

4.2.3.a What are the Gaussian Processes Morphable Models

In this subsection is introduced the theory behind the GPMMs. These models were introduced by Lüthi et al. and are explained in detail in a series of articles including [LFGV17, LGJV17]. In a first paragraph the mathematical concepts behind the models are introduced. Then in a second paragraph the models theory is described, along with various possibilities of covariance kernels and their effects for the model.

Gaussian processes

A *stochastic process* generalizes the concept of random variable. It is composed of a collection of random variables, which all take values from the same mathematical space. Often the random variables can be indexed by some mathematical set. A *Gaussian process* is a stochastic process composed of random variables, possibly an infinity of them, such that any finite subset of these variables follows a multivariate normal distribution. The Gaussian process distribution is the joint distribution of all its random variables, and as such is a distribution over functions with a continuous domain, for example space. This property is very interesting in the case of the GPMMs as it allows to describe shapes deformations as vector fields independently of the discretization. This is not the case with SSMs which are defined for a unique vertex distribution over the surface. A Gaussian process $\mathcal{GP}(\mu, k)$ is completely defined by its second-order statistics: its mean μ and its covariance k.

Let's consider the covariance function k of a Gaussian process $u_t \in \mathcal{GP}(0, k)$ for $t \in \Omega$, Ω is a subset of $\mathbb{R}^d$. A linear operator $\mathcal{T}_k$ is associated to k such that:

$$\begin{aligned} \mathcal{T}_k : L^2(\Omega) &\to L^2(\Omega) \\ f &\mapsto \mathcal{T}_k f = \int_\Omega k(s, \cdot) f(s) p(s) d(s) \end{aligned} \tag{4.7}$$

The eigenvalues and eigenfunctions pairs (λ_i, Φ_i) of the linear operator $\mathcal{T}_k$ are found by solving the equation:

$$\int_\Omega k(s,t)\Phi_i(s)p(s)ds = \lambda_i \Phi_i(t) \tag{4.8}$$

$p(s)$ is a density function defined on Ω. The *Karhunen-Loève theorem* states that a Gaussian process can be represented as an infinite linear combination of orthogonal functions $\{\Phi_i\}_{i=1}^{\infty}$, its covariance's eigenfunctions:

$$u \sim \sum_{i=1}^{+\infty} \alpha_i \sqrt{\lambda_i} \Phi_i, \quad \text{s.t. } \alpha_i \in \mathcal{N}(0,1) \tag{4.9}$$

On the opposite of other expansions, the orthogonal basis functions depend on the process, determined by its covariance function. The coefficients in the Karhunen-Loève theorem are independent Gaussian random variables $\{\alpha_i\}_{i=1}^{\infty}$. Due to the latter property, the eigenvalues λ_i explain the variance associated to the i^{th} component. Therefore, if the sorted λ_i decrease sufficiently quickly, a low rank approximation of u can be used:

$$\tilde{u} \sim \sum_{i=1}^{r} \alpha_i \sqrt{\lambda_i} \Phi_i \tag{4.10}$$

This approximation enables to get a parametric low-dimensional model from the Gaussian process. The associated error is given by:

$$\sum_{i=r+1}^{\infty} \lambda_i \tag{4.11}$$

The Karhunen-Loève theorem is closely related to the Principal Component Analysis, since the latter is also called Karhunen-Loève transform and is an empirical use of the Karhunen-Loève theorem.

The approximation (4.10) can only be used if the eigenvalues et eigenfunctions $(\lambda_i, \Phi_i)_{i=1}^{r}$ can be computed. Lüthi et al. propose to estimate the pairs using the Nyström method, which approximates the integral of (4.8). The integral over $p(x)$ is replaced by an empirical average over randomly sampled points $\{x_1, ..., x_n\}$, sampled according to p. It leads to a matrix eigenproblem:

$$K^{(n)} U^{(n)} = U^{(n)} \Lambda^{(n)} \tag{4.12}$$

with $K^{(n)}$ the kernel matrix such that $K_{ij}^{(n)} = k(x_i, x_j),\ i, j = 1, .., n$. The columns of $U^{(n)}$ are eigenvectors, $\Lambda^{(n)}$ is a diagonal matrix with the corresponding eigenvalues $\lambda_1 \geq \lambda_2 \geq ...\lambda_n \geq 0$. The Nyström approximation of the i^{th} eigenfunction is:

$$\Phi_i(y) \approx \frac{\sqrt{n}}{\lambda_i^{(n)}} k_y . u_i^{(n)} \tag{4.13}$$

with $k_y = (k(x_1, y), ..., k(x_n, y))$ and $u_i^{(n)}$ the i^{th} column of $U^{(n)}$. The eigenvalues $\lambda_i^{(n)}$ approximate the λ_is.

Gaussian Process Morphable Model

Gaussian Process Morphable Models are a generalization of more classical SSMs such as the PCA-based ones. The deformations undergone by a shape are modeled as a Gaussian process, which is fully characterized by its mean and covariance functions. Due to the Karhunen-Loève expansion of Gaussian processes and its resulting low-rank approximation, a parametric low-dimensional model describing the deformations can be computed, using the Nyström method.

It must be noted that PCA-based models are usually employed for modeling shapes variations using a normal distribution $\mathbf{x} \sim \mathcal{N}(\bar{\mathbf{x}}, C)$, $\mathbf{x}$ being a shape. However, instead of describing shapes, SSMs can model deformations undergone by the mean shape. Let Δ be the deformations modeled, then similarly to (4.6), $\Delta = wV^t\sqrt{\Lambda}$ and $\Delta \sim \mathcal{N}(0, C)$. The latter interpretation is the one used for GPMMs, the probabilistic model is defined directly on the deformations undergone by the mean shape. The generation of shapes from deformations simply consists in adding the mean shape to the deformations.

A Gaussian process is characterized by its mean and covariance functions. The functions defining the model must be carefully chosen, as they impart its specific properties. Some such properties can enforce smoothness, periodicity, symmetry, and so on. We will only discuss two kernels that are of interest for shape deformation modeling, but many more possibilities exist, either for modeling or other applications.

The first property that we are interested in is *smoothness* of the deformations. A very simple assumption consists in using a zero mean function. It implies that the reference shape that is being deformed is a representative instance of its class of shapes, close to a mean shape. Many different kernels can be used to enforce smoothness, one of the most classical one being a Gaussian kernel:

$$k_g(x, y) = s \cdot I_{3\times3} \cdot \exp(-||x - y||^2/\sigma^2) \tag{4.14}$$

$x, y \in \Omega \subset \mathbb{R}^3$, with $\Omega = S_R$, S_R being the reference surface that is being deformed. $s \in \mathbb{R}$ characterizes the scale of the deformation and σ defines the range of influence of a point. Finally, the identity matrix $I_{3\times3}$ signifies that the 3 dimensions of the vector field are independent.

This model incorporates no prior knowledge about a shape, and can therefore be applied to any shape, no matter its point distribution or the absence of a training shapes. However, when a set of valid shapes are available for training, it is ideal to learn valid deformations from them. We are therefore interested in a second time in *learning prior information from a training set*. If n valid shapes are in correspondence, deformation fields $\Delta_1, .., \Delta_n$ can be learned from the points locations, by subtracting the mean shape points positions. A Gaussian process $\mathcal{GP}(\mu_p, k_p)$ modeling these deformations can be computed:

$$\mu_p(x) = \frac{1}{n}\sum_{i=1}^{n} \Delta_i(n) \tag{4.15}$$

$$k_p(x,y) = \frac{1}{n-1}\sum_{i=1}^{n}(\Delta_i(x) - \mu_p(x))(\Delta_i(y) - \mu_p(y))^T \tag{4.16}$$

On the opposite of the Gaussian kernel, the deformation field is only known for the point distribution of the corresponding shapes.

The only requirement for a matrix to be a valid Gaussian process covariance function is that it should be symmetric and positive semi-definite. Algebraic rules define authorized operations between valid kernels to combine them into more complex ones. It enables the accumulation of various effects into complicated models. For example, a kernel resulting from a sum of Gaussian kernels with various s and σ values would allow multi-scale deformations, piling up global tendencies with finer and more local details. Other combinations can be used to make models more local or else to define partitions of the shape and apply various transformations depending on the section of the partition. More details about such combinations of transformations can be read in [LGJV17].

We are interested in making the most of the valid shapes available in the CMC database. However when the training set is limited, the span of shapes that can be represented by the model might not encompass the full shape space. In this case, the model is biased towards the training shapes. It is possible to reduce the bias by using a Gaussian kernel with parameter σ chosen large and s equal to the average error committed by the prior model alone, as studied in [LJV13]. It is based on the assumption that deformations are smooth and errors are spatially correlated. Therefore, we combine the prior learned from the training set in $\mathcal{GP}(\mu_p, k_p)$ with a Gaussian kernel $\mathcal{GP}(0, k_g)$. The new model is based on a Gaussian process $\mathcal{GP}(\mu_p, k_p + k_g)$

Another interesting property of a Gaussian process based model is the capacity to combine prior information and locations of some points given by a user to compute a new *posterior model*. Let Δ be the deformation modeled by a Gaussian process, describing the prior information:

$$\Delta \sim \mathcal{N}(M, K) \tag{4.17}$$

If Δ is in the form of a vector, describing the deformation for a point distribution then M and K are respectively a vector and a matrix. The most probable prior shape deformation is the mean vector M.

The user provides the actual deformations $\delta_{\text{obs}} = \{\delta_1, ..\delta_q\}$ of points $\{p_1, .., p_q\}$. Δ can be decomposed into two vectors Δ_Y and Δ_Z such that Δ_Z describes deformations for points $\{p_1, .., p_q\}$, while Δ_Y characterizes deformations for all the other points. M and K are decomposed accordingly:

$$\Delta = \begin{pmatrix}\Delta_Y \\ \Delta_Z\end{pmatrix} \sim \mathcal{N}\left(\begin{pmatrix}M_Y \\ M_Z\end{pmatrix}, \begin{pmatrix}K_{Y,Y} & K_{Y,Z} \\ K_{Z,Y} & K_{Z,Z}\end{pmatrix}\right) \tag{4.18}$$

Except if K is an identity matrix, points are related to each others and the movement of one point influences its neighbors. Δ_Y is modeled by a new Gaussian process taking the added posterior information δ_{obs} into account:

$$\Delta_Y|\delta_{obs} \sim \mathcal{N}(M', K') \tag{4.19}$$

such that:

$$\begin{aligned} M'(p) &= M(p) + K_{p,Z}\, K_{Z,Z}^{-1}\, (\delta_{obs} - \Delta_Z) \\ K'(p,p') &= K(p,p') - K_{p,Z}\, K_{Z,Z}^{-1}\, K_{Z,p'} \end{aligned} \tag{4.20}$$

The posterior model of the whole shape deformations is defined in eq. 4.21, and the most probable shapes are those characterized by the new mean.

$$\begin{pmatrix} \Delta_Y \\ \Delta_Z \end{pmatrix} \sim \mathcal{N}\left(\begin{pmatrix} M'_Y \\ \delta_{obs} \end{pmatrix}, \begin{pmatrix} K'_{Y,Y} & 0 \\ 0 & 0 \end{pmatrix} \right) \tag{4.21}$$

So far we have assumed that information given by the user are exact. It is however reasonable to suppose that it might be *noisy*. Indeed 3D shapes visualization on a computer is tricky and so is the definition of exactly corresponding points. Then the observed deformations $\tilde{\delta}_{\text{obs}} = \{\tilde{\delta}_1, .., \tilde{\delta}_q\}$ are such that

$$\tilde{\delta}_i = \delta_i + N, \qquad \text{s.t. } N \sim \mathcal{N}(0, \epsilon^2 I_{3\times 3}) \tag{4.22}$$

δ_i is the exact deformation for point p_i, $\tilde{\delta}_i$ is the observed one. N represents the noise and ϵ is a parameter to scale it. The prior model becomes:

$$\Delta_n = \begin{pmatrix} \Delta_Y \\ \Delta_Z \end{pmatrix} \sim \mathcal{N}\left(\begin{pmatrix} M_Y \\ M_Z \end{pmatrix}, \begin{pmatrix} K_{Y,Y} & K_{Y,Z} \\ K_{Z,Y} & K_{Z,Z} + \epsilon^2 I_{3q\times 3q} \end{pmatrix} \right) \tag{4.23}$$

and:

$$\Delta_n|\tilde{\delta}_{obs} \sim \mathcal{N}(M'_n, K'_n) \tag{4.24}$$

such that for any points p, p' of the shape, whether among the observed ones or not:

$$\begin{aligned} M'_n(p) &= M(p) + K_{p,Z}\, (K_{Z,Z} + \epsilon^2 I_{3q\times 3q})^{-1}\, (\delta_{obs} - \Delta_Z) \\ K'_n(p,p') &= K(p,p') - K_{p,Z}\, (K_{Z,Z} + \epsilon^2 I_{3q\times 3q})^{-1}\, K_{Z,p'} \end{aligned} \tag{4.25}$$

The GPMM describes the deformations of a shape. The training set is constructed from the matrix of shapes $\mathbf{X}$ defined in Sec. 4.2.2.a. The matrix is centered using $\mathbf{X_c}(i,j) = \mathbf{X}(i,j) - \bar{\mathbf{x}}(j)$ with $\bar{\mathbf{x}}$ calculated using (4.1). When a new deformation is simulated with the model, the equivalent shape is generated by summing the deformation and $\bar{\mathbf{x}}$. In the following section, such a model was computed with our data, we present the results.

4.2.3.b Applications

We test GPMMs for 3D shape registration towards the CMC database meshes $M_{D,\{b,i\}}$. The bones are considered separately, a model only describes one bone. The registrations are done in a leave-one-out manner: the target bone is systematically removed from the training set of the model. We use two distinct strategies to register the model to the target. First, we focus on the property of the Gaussian processes to adapt to posterior information. It is aimed at using external knowledge brought by a human user. In a second part, we will focus on an fully automatic registration method, similar to a SSM registration, based on deformation described by vectors.

Registration based on external inputs

One of the arguments in favor of a Gaussian process-based model is the exploitation of human knowledge, to fill in potential gaps of training data. Thus, we test a registration of models to new wrists completely based on external inputs. We have chosen to work with models based on a Gaussian process $\mathcal{GP}(\mu_p, k_p + k_g)$ combining knowledge from training data with the assumption that deformations are smooth. [LJV13] found out that it is an efficient covariance kernel for model registration.

The algorithm leading to model registration based on user input is:

1. $t = 0$: For a given target mesh $M_{D,\{b,i\}}$, the corresponding model $G_{\{b,i\}}(\mu_t, k_t)$ is computed by using all $M_{W,\{b,j\}}$, $j \in \{1, .., n\}, j \neq i$ as training set.
2. $M_{G\{b,i\}(\mu_t,k_t)}$ is aligned to $M_{D,\{b,i\}}$ using rigid + isoscale transformations.
3. The point $v_k \in G_{\{b,i\}}(\mu_t, k_t)$ with the biggest variance is computed based on k_t
4. **User input**: The desired location for one point of $M_{G\{b,i\}(\mu_t,k_t)}$, whether v_k or another one. The deformation is calculated from the position
5. $t = t + 1$: μ_t and k_t are updated according to (4.25)
6. $d_{\text{mean}}(M_{G\{b,i\}(\mu_t,k_t)}, M_{D,\{b,i\}})$ is computed using (**??**)
7. **User input**: "Ok" $\rightarrow$ End of the algorithm; "Nok" $\rightarrow$ Repeat 3. to 7.

$M_{G\{b,i\}(\mu_t,k_t)}$ is the mesh describing the most probable shape according to the model of shape deformation. It is simply the sum of the mean mesh and the mean deformation μ_t at time t.

The registration continues until the similarity of the shapes given by $d_{\text{mean}}(M_{G\{b,i\}(\mu_t,k_t)}, M_{D,\{b,i\}})$ is considered satisfying by the external user. The user can run the algorithm until he has manually given the positions of all points forming the model. In this extreme case any shape can be describe, if technically possible for the number of vertices. Hence even shapes very different from the ones in the training set can be described, such as degenerated ones due to sickness.

To begin with, this registration method is tested with a simulated ideal user. The coordinates given by the user are supposed exact. In step 5. μ_t and k_t are updated using (4.20). To give exact positions, it is assumed that the optimal registration of the model $G_{\{b,i\}}$ towards the target mesh $M_{D\{b,i\}}$ is equal to $M_{W,\{b,i\}}$. Additionally the user

systematically provides information about the vertex that has at the moment the greatest variance according to the model's kernel. Indeed it is the point for which there is the greatest uncertainty about its deformation, and potentially the most info to learn from: it is likely to influence a bigger area around it than another point with less variance.

The number of points needed from the user to reach some similarity levels are tested with the simulated ideal user. Three distances between the target mesh and the one stemming from the model are tested: 0.3, 0.25 and 0.2mm. 0.3mm is just below the original precision of the CT scans ($0.33 \times 0.33 \times 0.625$mm). Most individual PCA-based models reach a precision in range $[0.2; 0.25]$mm when they are registered to a new mesh. The registration was tested for all persons and all bones of the CMC database at turn in a leave-one-out manner. The minimum number of points required correspond with the number of iterations needed to drop below the similarity levels. The average minimum number of points are presented in table Table 4.1.

Distance max. btw. the meshes	< 0.3mm	< 0.25mm	< 0.2mm
Radius	37	53	80
Scaphoid	13	16	23
Lunate	11	15	23
Triquetrum	12	18	30
Pisiform	7	10	17
Trapezoid	11	16	28
Trapezium	17	26	43
Capitate	23	34	58
Hamate	20	29	48
Metac. 1	22	32	52
Metac. 2	29	45	78
Metac. 3	27	37	65
Metac. 4	23	33	56
Metac. 5	22	33	55

Table 4.1: Average minimum number of vertices required to reach level of similarity between a target mesh and a GPMM registered using only posterior information

While these numbers are not that high compared to the total number of vertices composing each bone (Table **??**), for some bones they are high when the time needed by an actual human being is considered, especially when a good similarity of shapes is expected. Manipulating 3D meshes on a 2D computer screen to accurately locate the target position of a point, even when helped by tools such as magnets is highly time consuming. The total time needed would be considerable for several tens of points. All the more so that Table 4.1 was computed in ideal conditions, a real user would probably need more points to reach the same similarity levels. With an actual human user, the algorithm would consider the information given as noisy. Moreover the user could decide to give locations of vertices that are more remarkable due to their location instead of filling in the ones with the most variance.

From this experiment, we conclude that a registration method completely based on human inputs is unrealistic. It requires too much time to be convenient in real conditions.

Automatic registration based on the Karhunen-Loève approximation

In a second time, GPMMs are being registered to a target mesh with an automatic optimization approach. The procedure is very similar to the PCA registration. It is aimed at comparing the results of the linear SSMs registration with ones, to compare the use of a linear model with

The registration is based on the low rank Karhunen-Loève approximation presented in (4.10). Any deformation can be approximated by a sum of vectors balanced by their associated eigenvalues and a vector α weighting the importance of each vector for the current deformation. These vectors are computed from the covariance function of the Gaussian process using the Nyström method. The automatic registration of the model to the target mesh is similar to the SSM registration: the values of α are optimized to minimize the difference between the target shape and the deformed template. We use the same procedure as the one presented in [LGJV17]. The parametric form of the registration problem is the following:

$$\alpha^* = \underset{\alpha}{\operatorname{argmin}} \; d_{\text{mean}} \left(\mathbf{x}_{\text{target}}, \bar{\mathbf{x}} + \mu + \sum_{i=1}^{r} \alpha_i \sqrt{\lambda_i} \Phi_i \right) + \eta \sum_{i=1}^{r} \alpha_i^2 \tag{4.26}$$

We did not have a chance to conduct an extensive review on GPMMs registration due to a lack of time. We have heavily based our experiment on the work of Lüthy et al. We have chosen to work with parametric models of 40 vectors, to have a comparable number of vectors than the SSMs, so comparisons make more sense. One model per bone was used. Our Gaussian processes were a composition of the estimation of an empirical model based on a training set and a Gaussian kernel to model the deformations smoothness. This composition was found to be the most effective one for registration in [LJV13]. Only one set of parameters for the Gaussian kernel was tested: in (4.14), σ represents the smoothness and was chosen large to model global deformations: $\sigma = 10$. s defines the scale of the average error, and was chosen to be $s = 0.5$. A leave-one-out approach was used, for two patients randomly selected. The average similarity between the optimized GPMMs and the target meshes are presented in Table 4.2. They are compared to the registration results of the SSMs for the two same patients.

The results in Table 4.2 show that both models are under the 0.3mm threshold, though the SSM ones perform better. However, the GPMMs have not been optimized at all, only one set of parameters were tested, and there's every chances that they are not the most appropriate ones. Additionally on the opposite of the SSMs, the number of modes used by the GPMMs could also be increased, it isn't limited by the size of the training set on the opposite of the linear model. Therefore, it can be expected that with optimal models the results could be improved.

	GPMM		SSM	
	d_{mean} (mm)	$d_{\text{Hausdorff}}$ (mm)	d_{mean} (mm)	$d_{\text{Hausdorff}}$ (mm)
Radius	0.268	2.950	0.236	1.460
Scaphoid	0.219	1.280	0.137	0.805
Lunate	0.144	0.738	0.132	0.871
Triquetrum	0.189	0.895	0.151	0.843
Pisiform	0.181	0.883	0.130	0.732
Trapezoid	0.223	0.987	0.161	0.765
Trapezium	0.242	1.078	0.156	1.104
Capitate	0.224	1.449	0.204	1.231
Hamate	0.220	1.429	0.201	1.123
Metac. 1	0.198	1.204	0.178	1.022
Metac. 2	0.225	1.798	0.184	1.668
Metac. 3	0.183	1.142	0.168	0.964
Metac. 4	0.190	1.063	0.151	0.840
Metac. 5	0.182	0.925	0.055	0.413

Table 4.2: Distance between the target mesh and the registered GPMM based on a distance minimization of the parametric model using 40 modes. Comparison with the registration of the SSMs based on 39 modes.

4.2.4 Discussion

In this section we have used the dense correspondence between bones of the CMC database previously computed to model the shapes variability. We have proposed two different models: one built with a PCA, another one based on Gaussian Processes.

The PCA-based models have proven to achieve good results for the registration of new shapes outside their training set, when a different model is used for each bone. The model describing the whole wrist at once couldn't replicate the shapes with a good enough level of details. The number of modes available, depending on the number of shapes in the training set was too poor to catch all the features.

In a second phase, Gaussian processes were used to model the variability of the deformations undergone by the mean bone shapes. They were then registered in turn to the database meshes, using two methods: one stepwisely incorporating posterior information from a user and one based on a parametric approximation of the Gaussian processes. The first approach has proven to require too many given points to be used on real conditions with a human user though a good similarity could be reached when enough information is provided. The second approach has not been extensively tested, but achieve similar results as the SSMs while the parameters have not been optimized. It is promising, and should be further studied.

The individual SSMs were quite effective to approximate new shapes. In the next section, they will be further tested by using them to register bones of a new database.

It is aimed at reparameterizing this second database to be in correspondence with the CMC one.

4.3 NIH reparameterization

In Sec. 4.2 were computed Statistical Shape Models using PCA. The registration results of the SSMs were promising, particularly the individual models which could approximate the CMC database meshes with a mean distance below 0.3 mm. These models were used to register the only publicly available wrist database: the NIH database [MCTL07].

Correspondence for the NIH database was not computed by using the same method than the one used for the CMC database introduced in Chapter **??**. Indeed, this database present additional difficulties: the radii and metacarpals are cut, and only small and variable portions of these bones are visible. It makes the alignment between the bones complicated, and if templates describe common information to all patients, it significantly limits knowledge to be learned from these bones, the carpal bones only are entirely known.

On the other hand, using the PCA-based SSMs computed with the CMC database to register the NIH database offers several interests. At first, as previously mentioned, a model quality is dependent on its training data diversity, and its assessment relies on the diversity of the test set. Therefore to have the possibility to test the model on more data from another database is an opportunity to further validate the model. Moreover if the results are good enough, the registered models can serve as a reparameterization of the NIH database. In this case the 60 wrists would be in dense correspondence with the CMC database, which would enable the use of both databases at once for the calculation of more complete models for instance. Or deeper shape analysis could be carried out due to the larger amount of data, since there is high chances that a larger span of wrists types are covered. Moreover, additional information can be learned from the models adjustments to the NIH bones: the CMC-based models encode complete metacarpals, and can be used as hints of what the whole bone shapes are like.

4.3.1 Dense correspondence mapping of the NIH using the SSMs

Similarly to the original meshes of the CMC database, the vertices of the raw meshes of the NIH database are irregularly spread along the bones surface (see Fig. **??**). This uneven distribution can skew the distance measures between meshes. A first step consists in resampling the bones to describe the shapes with the same number of vertices, but with an homogeneous distribution and a stable edge length. As previously, this resampling is computed using the graphite software [Lé], based on a Centroidal Voronoi Tesselation. These resampled homogeneous meshes are later on used as reference shapes. On the opposite of the post-segmentation processing that was performed on the first database, we did not need to remove coarse errors of segmentation.

To be able to adapt the statistical models to the bones, the latter have to be aligned to the former. Our optimization algorithm includes refinement of the rigid and scale alignment to the model at every iterations. However shapes of short radii are too different to the associated model, which makes basic shape alignment impossible, preprocessing is required. Six feature points were manually selected on all radii and metacarpals of the NIH database and on the mean models. The bones were then

roughly aligned to the models by minimizing the distances between sets of feature points. Additional adjustments could be manually done if needed. For each bone, the plane along which it had been cut was computed, and any vertex within one millimeter of the plane or beyond it was listed. A customized model was created for each bone by removing all recorded vertices, so both shapes would be similar. Vertices within one millimeter of the cut plane were also removed from the database meshes, these points being absent from the associated model. Carpal bones were roughly aligned by using the transformation matrix of the radii, it is enough to guarantee the convergence of the alignment algorithm.

Afterward, the models are being registered to the database bones. The latter are individual SSMs of each bone, computed with a training set of 42 wrists from the CMC database (please refer to Sec. 4.2.2). According to the mean shape, the eigenvectors and their associated eigenvalues, the best parameters to approximate each NIH bone are calculated. It was decided that 39 vectors would be used for the models, which is almost all available vectors. Indeed throughout the leave-one-out tests of the SSMs, it was proven that the more vectors are used, the better the results.

The SSMs of the radius and metacarpals describe the entire bones, however a portion only of the bone can be registered to the targets. All vertices of the SSM previously listed as beyond the cut plane for the current subject are therefore ignored during the distance computation. Moreover the refinement of the bone alignment by the optimization algorithm uses the customized model associated to the target, deformed in the same way than the SSM. Two radii of the NIH database had such a small part of them captured that they were discarded from the calculations.

In order to use the NIH database for further studies, we want to perfectly capture the details of the bones. Yet, if the results of the SSMs are comparable with the ones obtained with the leave-one-out method on the CMC database, we expect to correctly approximate the global shapes of the bones, but details should be missed by the registration. Therefore, in addition to the model registration via optimization of the parameters, a second step of projection along the normals is added. The same process was used when the CMC database was reparameterized (please refer to Sec. **??**). The shapes being already really close from each other, the points are not projected far, which prevents the meshes from having crossed faces or wrongly projected points. It allows to refine the registration by capturing the sharp details of the targets. All points listed as beyond the cut plane of the target mesh are removed from the final meshes, no corresponding target surface exists to project them onto.

Finally the resulting meshes are moved back to their target bones initial positions and orientations, to reconstruct the wrists. Two types of final wrists are available: the ones described by a deformation of the SSMs that include the whole metacarpals and a large portion of the radii, thanks to the extra information brought by the SSMs. The second type is composed of more precise meshes, that were projected onto the target surfaces, but only the portions of bones visible in the initial data are apprehended by the new meshes. Both types of wrists are in correspondence with the CMC database by construction. Only the similarity of shape between the database bones and the resulting meshes need to be validated, which is analyzed in the next section.

4.3.2 Numerical Validation

In the previous section was described the correspondence mapping of the NIH database with the CMC database. It was performed by optimizing individual SSMs previously created based on the second database to register the new one. In addition to the optimization of the SSMs, a second set of resulting meshes was created by additionally projecting the deformed SSMs towards the target bones. By construction all meshes of bone b for any subject are in correspondence with the ones of the CMC database, whether resulting from SSM deformation of further projection. To assess the quality of the correspondence mapping meshes, and to prove that they can be used instead of the original raw meshes, only the similarity of the encoded shapes needs to be evaluated.

NIH resampling

At the very first, the NIH database has been resampled, to be described by an homogeneous distribution of points over the surface. The treatment is the same than the one applied to the CMC database. Similarly, this step is very important, since the resulting meshes are used as reference for the rest of the work. If differences are introduced during this step, they will remain in the data. Therefore particular attention is paid to achieve proper outcomes.

In Table 4.3 the results of the resampling step are introduced. Dissimilarity between meshes is computed using two mesh-to-mesh distances: a mean distance from a vertex to its closest point on the paired surface (**??**) and a max distance, which corresponds to the maximal distance over all vertices of both meshes of a vertex to its closest point (**??**). The mean distance between a vertex and its closest point is in average between 0.002 and 0.004 mm and the maximal values are included in range $[0.004; 0.007]$ mm. The Hausdorff distance is in average between 0.026 and 0.078 mm, while its maximal values are under 1.5mm, that is below the acquisition precision. Only one 1^{st} metacarpal has a maximal value of 0.201mm, slightly above the 0.2mm threshold. After verification, this higher value is due to small holes in the original mesh next to the cut plane that are mishandled by the algorithm. However since the holes are really close to the cut plane, they will not be taken into account in the following processes, and the distal side of the bone is not affected, so it was kept in the database

The results are in the same order of magnitude as the resampling results of the CMC database, perhaps even slightly better (please refer to Sec. **??** for the CMC database results). The precision of the initial data is between $0.2 \times 0.2 \times 1$ and $0.3 \times 0.3 \times 1$ mm. The distance between a vertex and the paired surface is in average largely below the precision of the raw data. Even in maxima, this distance is always below the initial precision, but for one bone. Given these distances, we can conclude that the resampled data perfectly characterize the original shapes of the NIH database.

SSMs mean shapes

In Table 4.4 are presented the distances between the individual SSMs mean shapes and the meshes of the NIH bones, when the bones have been rigidly aligned and scaled.

	Mean dist. (??)			**Hausdorff dist. (??)**		
	mean	max	std	mean	max	std
Radius	**0.004**	0.005	0.001	**0.078**	0.133	0.020
Scaphoid	**0.003**	0.004	0.000	**0.043**	0.068	0.009
Lunate	**0.003**	0.004	0.000	**0.038**	0.069	0.009
Triquetrum	**0.002**	0.005	0.000	**0.037**	0.073	0.010
Pisiform	**0.002**	0.004	0.001	**0.026**	0.069	0.009
Trapezoid	**0.003**	0.004	0.000	**0.039**	0.070	0.009
Trapezium	**0.003**	0.004	0.000	**0.040**	0.057	0.008
Capitate	**0.004**	0.005	0.001	**0.051**	0.084	0.010
Hamate	**0.003**	0.004	0.000	**0.050**	0.069	0.008
Metac. 1	**0.003**	0.006	0.001	**0.060**	0.201	0.029
Metac. 2	**0.004**	0.007	0.001	**0.064**	0.125	0.018
Metac. 3	**0.004**	0.007	0.001	**0.060**	0.101	0.017
Metac. 4	**0.003**	0.006	0.001	**0.048**	0.078	0.012
Metac. 5	**0.003**	0.006	0.001	**0.052**	0.104	0.018

Table 4.3: Distances between the original meshes and a first resampling to regularize the vertices and edges distribution on the surface of the NIH bones. Both mean and Hausdorff distances (**??**) and (**??**) are computed, the results are in mm.

These distances are for comparison with later results of the SSMs registration. It enables to measure the quality of the registration compared to the initial situation.

The average distance between a vertex and the paired surface is included in range $[0.311; 0.747]$ mm, and the worst values go as high as 0.591 to 1.673 mm. In average the surfaces are far from each other, the global shapes aren't captured by the mean shape. It proves the variability of shape among the same class of bones. The Hausdorff distances are in average between 1.218 and 2.779 mm, while the maximal values of the Hausdorff distance are for some bones higher than 5 mm, even up to 7.038 mm for a 1^{st} metacarpal. Compared to the size of the bones, these distances are really high. These results are in the same order of magnitude as the difference between the CMC database meshes and the initial templates visible in **??**. They are slightly worse for the metacarpals and the radii, due to the cut ends of the bones, although the distance functions have been modified to take these into account.

SSMs registration

When the bones are aligned and scaled to the individual SSMs, the latter are being deformed following their principal modes of variations. They are being registered to the database meshes by optimization of a mean distance function. The resulting registered SSMs are being compared to the database meshes. All vertices of the models that have been identified as having no equivalent target surface are ignored in the distance computation. The average mean distances are included between 0.117 and 0.195 mm, while the highest mean distances are in range $[0.165; 0.305]$ mm. The Hausdorff distances are

	Mean dist. (??)			**Hausdorff dist. (??)**		
	mean	max	std	mean	max	std
Radius	**0.747**	1.673	0.275	**2.779**	7.038	1.003
Scaphoid	**0.373**	1.022	0.123	**1.758**	4.431	0.700
Lunate	**0.411**	1.142	0.184	**1.557**	2.943	0.482
Triquetrum	**0.320**	0.624	0.082	**1.280**	1.936	0.286
Pisiform	**0.311**	0.591	0.089	**1.218**	2.129	0.295
Trapezoid	**0.345**	0.884	0.120	**1.416**	2.421	0.416
Trapezium	**0.362**	0.875	0.127	**1.508**	4.221	0.553
Capitate	**0.417**	1.162	0.167	**2.011**	4.489	0.771
Hamate	**0.382**	1.202	0.171	**1.656**	4.846	0.665
Metac. 1	**0.566**	1.354	0.219	**2.726**	7.459	1.582
Metac. 2	**0.556**	1.372	0.180	**2.070**	4.064	0.642
Metac. 3	**0.457**	0.964	0.143	**1.939**	5.195	0.717
Metac. 4	**0.448**	1.153	0.158	**1.806**	5.448	0.939
Metac. 5	**0.422**	0.796	0.110	**1.549**	3.570	0.514

Table 4.4: Distances between the NIH database meshes and the SSMs mean shapes. Both mean and Hausdorff distances (**??**) and (**??**) are computed, the results are in mm.

included between 0.575 and 1.039 mm in average and between 0.879 and 2.599 mm for the maximal values.

When the registered SSMs are being compared to the mean shapes, we can observe that they are strictly closer to the target meshes, as expected. We can also note that in average the mean distance between a vertex and the paired surface is smaller than the initial precision of the data, though some of the highest mean distances are above the 0.2 mm threshold, which is the best original precision of some of the original data. We can however conclude that the global shape is well captured by the deformed models. However the Hausdorff distances for their part are quite high, details are definitely missed. These distances can be compared to the distances obtained between individual models registered using 39 principal modes to the CMC database bones, in Fig. 4.3 and Fig. 4.4. The results are slightly better for the NIH registration than they were with the leave-one-out method for the CMC database registration.

We can note that the SSMs of the metacarpals, created based on the CMC database, represent the whole bones, while they are being registered to the proximal end of the bones only. This has both upsides and downsides. The model is not exactly adapted to the data it must describe. Some of its modes could characterize shape variations in the distal end of the bone only, which could therefore give absurd values associated to these modes. Since the models are not perfectly fitting the data, it is one of the reason why the results are somewhat worse for these bones. The same apply to the radius, which portion of diaphysis available in the model is far longer than the ones in the NIH database radii. We could imagine to learn the models only for the length of the bone visible in the target mesh. The model would therefore be more adapted. However, in

	Mean dist. (??)			**Hausdorff dist. (??)**		
	mean	max	std	mean	max	std
Radius	**0.195**	0.304	0.037	**1.039**	2.526	0.283
Scaphoid	**0.137**	0.191	0.020	**0.670**	0.999	0.123
Lunate	**0.123**	0.191	0.019	**0.638**	1.013	0.129
Triquetrum	**0.123**	0.165	0.015	**0.622**	0.879	0.108
Pisiform	**0.117**	0.208	0.040	**0.575**	1.533	0.207
Trapezoid	**0.144**	0.305	0.039	**0.744**	1.320	0.195
Trapezium	**0.152**	0.197	0.019	**0.766**	1.328	0.155
Capitate	**0.173**	0.236	0.022	**0.908**	1.409	0.158
Hamate	**0.167**	0.250	0.027	**0.910**	1.583	0.198
Metac. 1	**0.139**	0.211	0.030	**0.710**	1.293	0.152
Metac. 2	**0.175**	0.227	0.024	**0.996**	2.599	0.292
Metac. 3	**0.151**	0.202	0.023	**0.783**	1.214	0.179
Metac. 4	**0.133**	0.182	0.017	**0.690**	1.222	0.142
Metac. 5	**0.121**	0.165	0.017	**0.611**	0.905	0.127

Table 4.5: Distances between the NIH database meshes and the registered SSMs. Both mean and Hausdorff distances (**??**) and (**??**) are computed, the results are in mm.

exchange of a model less customized to the target shapes, we gain information about the distal end of the bone that is not initially present in the database. The models bring additional knowledge.

Projection towards the target meshes

As previously analyzed, the deformed SSMs capture the global shapes of the bones, but miss details. If we want to enrich our data by mixing both NIH and CMC database, we need to fully trust the shapes characterized by the corresponding meshes. Therefore the shapes describing the NIH bones were refined by projecting the vertices towards the target surface, as previously done with the CMC data.

In Table 4.6, the distances between target bones and final meshes are presented. The mean distances between the shapes are smaller than 0.035 mm for all bones. This is largely below the initial precision if the data. The Hausdorff distances are included in range $[0.174; 0.295]$ mm with highest values up to 0.565 mm. The highest distances between vertices and the paired surface are a little higher than the original precision of the data. However, these distances are small nonetheless, half a millimeter at worst, and concern a few vertices at max. The data can be trusted to be used instead of the initial meshes.

4.3.3 Discussion

In this section, by using the statistical shape models constructed based on the CMC database, we have been able to reparameterize a second database and map it to be

	Mean dist. (??)			**Hausdorff dist. (??)**		
	mean	max	std	mean	max	std
Radius	**0.015**	0.019	0.002	**0.287**	0.565	0.096
Scaphoid	**0.020**	0.025	0.002	**0.221**	0.458	0.067
Lunate	**0.018**	0.021	0.001	**0.199**	0.315	0.047
Triquetrum	**0.023**	0.028	0.002	**0.230**	0.347	0.047
Pisiform	**0.019**	0.024	0.002	**0.185**	0.359	0.050
Trapezoid	**0.020**	0.025	0.002	**0.255**	0.517	0.081
Trapezium	**0.029**	0.035	0.003	**0.295**	0.533	0.071
Capitate	**0.019**	0.023	0.002	**0.222**	0.362	0.048
Hamate	**0.022**	0.028	0.002	**0.283**	0.431	0.069
Metac. 1	**0.013**	0.019	0.002	**0.174**	0.423	0.071
Metac. 2	**0.018**	0.024	0.003	**0.216**	0.363	0.062
Metac. 3	**0.020**	0.030	0.004	**0.257**	0.417	0.067
Metac. 4	**0.020**	0.031	0.004	**0.208**	0.360	0.058
Metac. 5	**0.018**	0.029	0.003	**0.177**	0.340	0.049

Table 4.6: Distances between the NIH database meshes and the final resulting meshes. Both mean and Hausdorff distances (**??**) and (**??**) are computed, the results are in mm.

in dense correspondence with the first one. We have proven that the shapes of the raw meshes and the final projected ones are very similar and can be used instead of each other. We haven't tested the quality of the correspondence between the vertices. However, the meshes were constructed by deformation of statistical shape models following their principal modes. By construction, they are in dense correspondence. It should also be noted that during the registration of the SSMs of complete bones to the only proximal end of these bones, we added information about the distal end of the metacarpals that is absent from the initial data. However, during the projection step, only vertices having close neighbors were projected. The parts with no initial information could obviously not be refined. This step loses the extra knowledge brought by the former process. In the case where this info would be needed, the meshes output by the SSMs registration have to be used.

Since the SSMs were able to register properly the target meshes, it proves that they are not too specific to the training set. An additional step of projection of the vertices towards the target surface was used to refine the results. The final shapes are very close to the target ones, we can use them instead of the original meshes. Additionally, by construction, the correspondence is guaranteed, the NIH database is now in correspondence with the CMC database. In future studies it will enable the use of all patients from both databases, which doubles the number of wrists considered. Issues had to be faced about the metacarpals and radii bones due to a variable length of bones visible in the NIH database, while longer portions were encoded in the SSMs.

The two first sections of this chapter are dedicated to te construction of statistical models, and their registration to 3D shapes. This is mostly aimed at testing the quality

of the models before using them for registration to images. In the following section, a completely different domain of application is proposed: biomechanics and definition of system of coordinates for joint movement measurement.

4.4 Anatomical Joint Coordinate Systems

In this section, we are interested in the computation of a joint coordinate system for the trapeziometacarpal (TMC) joint. Joint coordinate systems are a common tool for the analysis of joint kinematics. They are composed of two coordinate systems, one attached to each bone of the joint. The description of a motion is based on the rigid movement of the distal bone with respect to the proximal one. We are concerned with the TMC joint, the articulation situated at the base of the thumb, connecting the trapezium and the 1^{st} metacarpal, as shown in Fig. 4.7a. But we argue that once the method has been proven reliable for this joint, it can naturally be transferred to any other wrist articulation.

The computation of anatomical coordinate systems offers a dual benefit for our work: our method is completely based on the correspondence relations between the meshes $M_{W,\{b,i\}}$ previously computed. The quality of the results fully depend on the quality of the corresponding points locations. We prove that we get equivalent results to another analytical specialized approach, we therefore consider it an evidence that the corresponding meshes are to be trusted. Additionally, our method is general and naturally functional for any other joint. We illustrate that the database that has been put in correspondence can have many applications in various domains. While in the previous sections we were focused on shape models for 3D shape registration, we are now concerned with a biomechanical utilization.

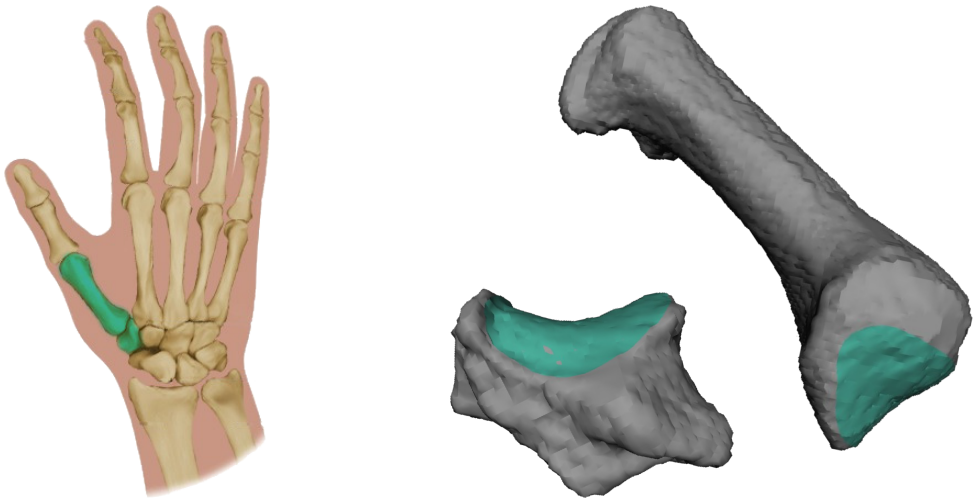

(a) The location of the TMC joint in the wrist

(b) The articulation surfaces of the TMC joint. The two bones are differently scaled for visualization purposes.

Figure 4.7: The TMC joint

4.4.1 State of the art

The unique versatility of the human hand is due to its opposable thumb, essential for dexterity as well as for effective handling [JL06]. These skills rely on the thumb's large range of motion [CLCL81], enabled mostly by the trapeziometacarpal joint . This articulation is also one of the joints the most affected by osteoarthritis [MvdWN+10],

which can prove to be disabling in everyday life. For these reasons, it is important to study the thumb and the TMC joint. Several previous works have addressed the TMC joint kinematics ([HRG+14], [CHM+15], [KOT+18]). It is an intricate joint, composed of saddle-shaped articular surfaces, as shown in Fig. 4.7b. The two main mechanical axes for extension-flexion and abduction-adduction are nonorthogonal and nonintersecting ([HBM+92], [CHM+15]).

Studies of joints motions require the definition of geometrical reference systems in order to describe the bones kinematics. A strong condition to define such a system is the necessity of reproducibility. Multiple reference systems for the TMC have been proposed in the literature, as more appropriate systems allow to be more precise in the kinematics description. In particular, axes parallel to the direction of movement are ideal, though they are also required to be easily reproducible.

Cooney et al. [CLCL81] were among the first ones to propose a joint reference system for the TMC. The definition of the system is based on the location of anatomical landmarks identified during a cadaver study. It is composed of a fixed coordinate system on the trapezium and a moving one on the 1^{st} metacarpal. In [WC95], the International Society of Biomechanics (ISB) issued global recommendations on the definition of joint coordinate systems. In [WVdHV+05] the ISB proposed system definitions for the joints of the human upper body, among which the wrist and the TMC joint. The axes of the carpal bones are to be parallel with the ones of the radius. The TMC joint coordinate system is defined separately: it is to be the same as the one proposed by Cooney et al [CLCL81], but the axes order is changed.

Cheze et al. [CDC+09] refined the ISB system, their axes becoming more coherent with the thumb main degrees of freedom. However their joint reference systems are still based on anatomical landmarks and are thus subjected to variability for their identification. Variability due to landmark identification was studied by Della Croce et al. [DCLCC05]. They addressed the errors committed through the selection of landmarks and reported their effects on the reliability and interpretation of joint kinematics. They advise for the use of more robust methods, based on automatic image processing for instance.

Coburn et al. [CUC07] introduced automatically computed coordinates systems for all wrist bones, based on the bones inertial axis. While easily reproducible, these axis are dependent on the bones global shape, and might be subjects to variations on the axis directions across wrists. Typically, a change of shape away from a joint surface may influence the location of the axes, making them less representative of the joint morphology. These axis also don't follow the ISB recommendations [WC95].

The latest proposal for TMC joint coordinate system computation is a semi-automated method introduced by Halilaj et al. [HRG+13]. It is based on the saddle-shaped articular geometry of the TMC joint (Fig. 4.7b). The articular surfaces of the trapezium and 1^{st} metacarpal are manually selected, then fit with fifth order polynomial surfaces. Using the approximation, the principal directions of curvature of the articular surfaces are computed. The coordinate systems origins are the two saddle points, one on each bone. The axis are oriented along the principal directions of curvature of the saddles. The polynomial approximation and the definition of the axis from the principal directions

of curvature make the method very specific to local geometry and the saddle-shaped articulation. At the same time, it has been proven that the actual kinematic rotation axis for extension-flexion and for abduction-adduction movements are not always the main directions of curvature of the saddle ([HBM+92], [CHM+15]).

We propose an alternative approach of axis computation based on correspondence between meshes. The joint coordinate system is the one defined by Halilaj et al [HRG+13], based on the geometry of the articular surfaces of the articulation. We show that similar performances as [HRG+13] are achieved for the TMC joint, while having some additional benefit. Typically, the approach has the advantage of being easily adapted to any other system definition on any bone. No limitations to inertial description or local surface approximation allows definition of truly mechanically meaningful coordinates systems. However, we focus on the TMC joint because a comparison can be drawn with the proven approach of [HRG+13]. We evaluate the anatomical relevance of the correspondence mapping method for the TMC joint thanks to a comparison to [HRG+13].

4.4.2 Coordinate System Computation

One of the key condition for joint coordinate systems definition is the reproducibility. It is therefore expected that if a system is defined for one instance of a shape class, we should be able to define the anatomically corresponding system on all other instances. Previous methods were either based on landmarks [CLCL81, WVdHV+05], but it is a source of variability [DCLCC05], or based on analytical analysis of the shapes [HRG+13]. Our method reproducibility capacity rests on correspondence between shapes.

We work with the meshes $M_{W,\{b,i\}}$, for which we have already computed correspondence relations (Chap. **??**). They are such that each k^{th} vertex of bone b mesh is localized on the same anatomical point of the class across the instances (Sec. **??**). Our method expects at least one instance of a coordinate system to be known originally. Then the example(s) is(are) transferred to all other instances:

The *origin of the system* is a point on the shape surface. It is either a vertex of the mesh, or a point of one of the mesh faces. In the case of a unique example, if the origin point is a vertex on the example shape, then the same vertex is the origin of the systems for all instances. It stems from the mesh correspondence properties that they are anatomically equivalent. If the example origin point is on one of the faces, its relative position on this face is computed. All origins are then located in the same position of this face, relatively to the face vertices. In the case of multiple examples, we expect the origins to be either all on the same face, or at least to be on neighboring faces. Otherwise, it would mean that the examples are already anatomically dissimilar. Let t_R be the triangular face on which the most centers are. t_R defines for each mesh a plane onto which the example centers are projected, the projection coordinates being expressed relatively to t_R vertices. The mean projected coordinates determine the coordinate system's center relatively to t_R vertices, and can be computed for every other database subjects.

The *vectors of the system* can be computed based on various properties. It can either rest on the correspondence property of the meshes, similarly to the origin definition.

The vectors orientations are expressed relatively to the plane defined by the face the origin belongs to. These orientations are copied for all other coordinate systems. In the case of multiple original examples, the average orientation is transferred. Or their computation can more generally rely on global properties of 3D meshes. For instance, Halilaj et al have to approximate the shape of the articulation surface to compute the principal directions of curvature. Yet curvature tensors could also be estimated from the mesh surface ([CSM03]) to compute the principal directions of curvature, once the saddle point has been defined.

This method requires no other knowledge than at least one example of a system, when the database is in correspondence. Such an example can be algorithmically computed or be given by a user. The definition is free of a mathematical or algorithmic description that must work in all cases, and is independent of landmarks. It can therefore be customized to match as well as possible the actual biomechanical axis of rotation, which are not exactly the main directions of curvature of the articulation surface in the case of the TMC joint. The results can be improved by inputting multiple examples, to limit the potential errors committed both during the definition (external to our method) and the transfer phases. It is therefore recommended to define numerous example systems, though one is theoretically enough.

4.4.3 Comparison with Halilaj's results

In [HRG+13], Halilaj and his team introduced a joint coordinate system for the TMC articulation. It is composed of two coordinates systems called Segment Coordinate Systems (SCS) defined on the trapezium (`TPM`) and the first metacarpal (`MC1`) bones. We compare the results of the SCS computation using their analytic procedure (that we call A-SCS) with our own method, based on mesh coherence across the subjects (named M-SCS).

To test our method, we annotated the saddle points of 15 randomly chosen subjects, for both articular surfaces of the `TPM` and `MC1`. From these examples, we estimated the M-SCS locations for all database meshes. Multiple options were viable for the vectors computation. However, we are mostly interested in the evaluation of the correspondence quality between the meshes, and therefore chose to rely on the correspondence property for the axis calculation. The orientations of the example SCSs relatively to the mesh surface are transferred to the other subjects.

As in [HRG+13], the steadiness of the M-SCS systems origins and orientations across the database is evaluated. The database bones are all aligned and scaled using ICP. Inter-subject variability is defined as the difference between individual M-SCS's locations and the average one, as well as the difference of orientation between each axis and the average one. The measure of a single angle between each individual system and the average one are also given, a global angle provides more information. The SCS systems using the analytical method were also computed, and we compare the results of the two approaches.

The difference of location and orientation between individual and average M-SCS systems are presented in Table 4.7a. Globally both location and orientation results are

slightly better for TPM bones than for MC1 ones. The mean location distances are of 0.59 mm for TPMs with a maximum value of 1.15mm, and for MC1s, the mean distance is 0.76 mm with a maximum of 1.43mm. The global angles between the systems orientations are 4.3°on average for TPM bones, the highest difference being 11.7°and those values are 6.1°and 11.5°for the MC1 bones.

Those values are compared with the ones obtained by computing A-SCS systems on our database. Both systems give results in the same order of magnitude. M-SCS gets slightly better results for the TPM bone, especially for the origin locations, with a mean error of 0.59 mm versus a mean error of 0.81 mm using A-SCS. On the opposite A-SCS get slightly better results for the MC1 origin locations. However the orientation are steadier for both bones using the correspondence based method, while the magnitude of errors remain the same.

An example of an SCS system can be observed in Fig. 4.8 for both TPM and MC1 bones.

		Location (mm)	**Orientation (°)**			
			X axis	Y axis	Z axis	Global angle
TPM	mean	**0.585**	**3.477**	**3.533**	**3.241**	**4.327**
	max	1.149	7.298	11.714	9.128	11.673
	std	0.237	1.647	2.056	1.777	1.961
MC1	mean	**0.762**	**4.901**	**5.068**	**4.378**	**6.109**
	max	1.434	8.856	11.509	9.072	11.541
	std	0.299	1.979	2.354	2.451	2.192

(a) SCS steadiness when computed with our correspondence-based method

		Location (mm)	**Orientation (°)**			
			X axis	Y axis	Z axis	Global angle
TPM	mean	**0.814**	**6.293**	**5.353**	**4.864**	**6.987**
	max	1.463	16.189	16.589	11.456	17.086
	std	0.315	3.455	3.104	2.570	3.347
MC1	mean	**0.706**	**5.747**	**5.121**	**6.315**	**7.280**
	max	1.614	10.773	10.468	11.091	12.425
	std	0.334	2.885	2.351	2.932	2.782

(b) SCS steadiness when computed with [HRG+13] analytical method

Table 4.7: Comparison between the analytical method of [HRG+13] and ours : study of the inter-subject variability of the joint coordinate systems location and orientation for the TPM and MC1 bones.

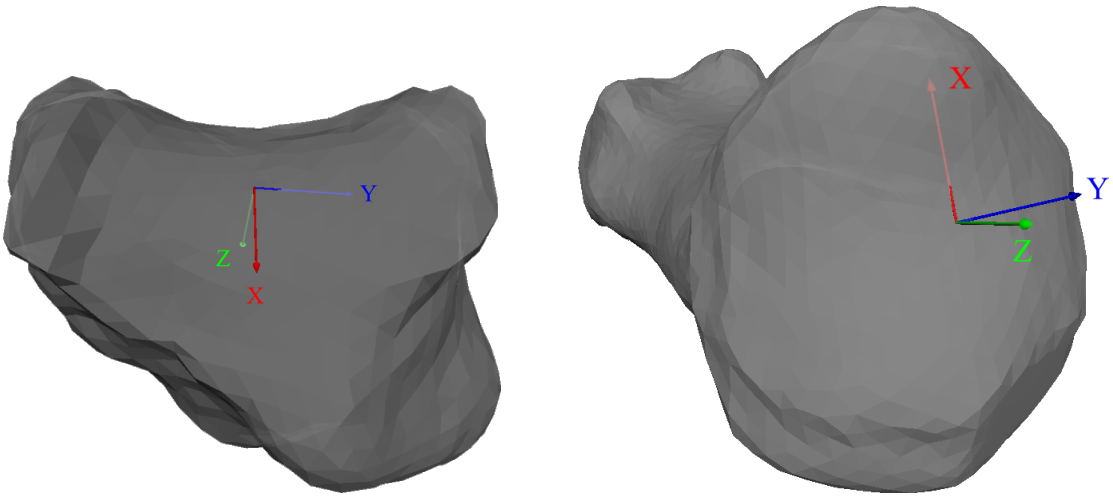

Figure 4.8: Examples of coordinates systems defined by [HRG+13] and computed with our method, for the `TPM` (left) and `MC1` (right) bones of a patient.

4.4.4 Discussion

We have proposed a method that is able to reproduce coordinate systems for all bones of our database when one or a few examples have been defined. The method rests on the correspondence relations between the meshes. We have tested it using a joint coordinate system definition given in [HRG+13] for the TMC articulation. Systems based on this definition were computed using both their analytical method and our correspondence-based one. We prove that the steadiness of the systems are in the same range of values using both approaches, even slightly better for our procedure. Our method is completely based on the quality of the correspondence relations previously created, and gets equal results than another very specialized method. We deduce that the correspondence between meshes is to be trusted.

We have equivalent results than a local specialized method that is fit to compute one definition of coordinate systems for one articulation only. Yet our approach uses no prerequisite that makes it specific neither to this articulation nor to this particular system definition based on principal curvatures. Any system described by a user on one or a few examples can be reproduced on any bone, for instance systems that are better adapted to the TMC joint. It has indeed been proven that the principal directions of curvature of the saddle-shaped surfaces of the TMC joint are not the actual kinematic rotation axis ([HBM+92], [CHM+15]). Any other wrist joint can be examined as well. We could imagine for example to define multiple joint coordinate systems to study the entire articular chain of the thumb in the wrist, including the radius and the scaphoid as suggested by [DDK+17].

This mapping of bones through dense correspondence can also have other applications. For example the location of the ligaments attachment to bones can naturally be transferred from one subject to all other. Simulations of tendons adapting to various shapes of wrist bones could be imagine as a possible application.

4.5 Conclusion

In this chapter we have proposed different applications of the database that was previously put in dense correspondence: the meshes can be used to create statistical models which can in turn be used to compute correspondence for new instances of the shapes, even when the latter are incomplete. The correspondence relations can also be used to transfer landmarks or coordinate systems from one or a few examples to all other occurrences of the database.

First we have studied the precision level that could be reached by statistical models for 3D shape registration. PCA-based models representing one bone have proven to be able to reach a good similarity with the target mesh, the mean error is below the precision of the original data. They have been further tested on a new database and enabled to reparameterize the latter to be in correspondence with the meshes of the first database. We have chosen to use an additional step of projection of the optimized models towards the target meshes. It was aimed at warping as well as possible the NIH meshes in order to use them later as training shapes with certainty that they faithfully represent the bones.

PCA-based statistical models were defined both for all wrist bones at once and for each bone separately. While the individual models have been shown to reach a good level of precision for 3D shape registration, the global model wasn't precise enough for the whole wrist registration. It is interesting to consider all bones at once, as they are really close from each other and the shape of one bone necessarily influences its neighbors shapes. However, the model has proved to need more principal modes than were available from the training set formed with the CMC database. Now that the NIH database is in correspondence with the CMC one, more data are available, a possible perspective would be to compute a new model for the whole wrist using both databases together as prior information. In addition to a larger span of shapes learned, more modes would be available, which could enable the model to reach a higher level of registration precision.

A second type of models were used: Gaussian Processes Morphable Models. Shapes are modeled as vertex deformations undergone by the mean shape. These models are promising: depending on the covariance function chosen, they can have various combined properties, and are not necessarily linear. Moreover, they adapt to posterior information, which allows human intervention in the results. A completely user-based registration approach was tested and was successful, really high similarity levels between shapes that can be reached as long as enough points are given by the user. However, we have concluded that in real-life the algorithm cannot be used as is, it would require too much points hence too much time from a qualified person. In a second phase an all-automatic registration method based on a parametric approximation was tested, and achieved good results. They were not as good as the SSMs ones, but lack of time prevented us from optimizing the model parameters, and we believe that better similarity can be reached. We believe GPMMs to be promising and next steps would be to further test the model and maybe mix the all-automatic and all-user based methods.

Statistical models can have various utilizations. For example they can be employed for a quantitative analysis of bone shapes and allow the identification of phenotypes [CLW+14]. They are often used as prior knowledge for image segmentation [CGHM12, ARJ+14]: the models are being registered to the 2D or 3D images and provide simultaneously a segmentation of the object in the image and a 3D representation of it. Such applications are dependent on the quality of the model and its capacity to represent new shapes. Now that it has been assessed that the SSMs are quite precise, these applications could be implemented.

Finally a biomechanics oriented application was proposed. We have shown that based on the correspondence relations previously established, landmarks and vectors can be easily transferred from one or a few instances of the database to all others. We have proven that the reliability of our method is similar to another method proposed in the litterature. This method happens to be to the best of our knowledge the only automatic method of joint coordinate system definition for the TMC joint, except for the method proposed in [CUC07] which doesn't follow the ISB prescriptions. Our method is less specialized than the one it was compared to and can therefore be employed on any other articulation of the wrist. It can also be used for any other application requiring the transfer of points to other instances of a same shape. Additionally the reliability of the method was a proof of the quality of the correspondence relations defined in the previous chapter.

This chapter and the last one's purpose was to study the wrist bone shapes. In the next chapter we will present the work we have done about wrist movement. The ultimate goal is to be able to take a wrist phenotype into account when its movement is modeled.

BIBLIOGRAPHY

[ARJ+14] Emran Mohammad Abu Anas, Abtin Rasoulian, Paul St John, David Pichora, Robert Rohling, and Purang Abolmaesumi. A statistical shape+ pose model for segmentation of wrist ct images. In *Medical Imaging 2014: Image Processing*, volume 9034, page 90340T. International Society for Optics and Photonics, 2014.

[BV+99] Volker Blanz, Thomas Vetter, et al. A morphable model for the synthesis of 3d faces. In *Siggraph*, volume 99, pages 187–194, 1999.

[CDC+09] Laurence Cheze, Raphaël Dumas, Jean-Jacques Comtet, Claude Rumelhart, and Michel Fayet. A joint coordinate system proposal for the study of the trapeziometacarpal joint kinematics. *Computer methods in biomechanics and biomedical engineering*, 12(3):277–282, 2009.

[CGHM12] Xin Chen, Jim Graham, Charles Hutchinson, and Lindsay Muir. Automatic inference and measurement of 3d carpal bone kinematics from single view fluoroscopic sequences. *IEEE transactions on medical imaging*, 32(2):317–328, 2012.

[CHM+15] Joseph J Crisco, Eni Halilaj, Douglas C Moore, Tarpit Patel, Arnold-Peter C Weiss, and Amy L Ladd. In vivo kinematics of the trapeziometacarpal joint during thumb extension-flexion and abduction-adduction. *The Journal of hand surgery*, 40(2):289–296, 2015.

[CHTH94] Timothy F Cootes, Andrew Hill, Christopher J Taylor, and Jane Haslam. Use of active shape models for locating structures in medical images. *Image and vision computing*, 12(6):355–365, 1994.

[CLCL81] William P Cooney, Michael J Lucca, EY Chao, and RL Linscheid. The kinesiology of the thumb trapeziometacarpal joint. *J Bone Joint Surg Am*, 63(9):1371–1381, 1981.

[CLW+14] Abhijit J Chaudhari, Richard M Leahy, Barton L Wise, Nancy E Lane, Ramsey D Badawi, and Anand A Joshi. Global point signature for shape analysis of carpal bones. *Physics in Medicine & Biology*, 59(4):961, 2014.

[CSM03] David Cohen-Steiner and Jean-Marie Morvan. Restricted delaunay triangulations and normal cycle. In *Proceedings of the nineteenth annual symposium on Computational geometry*, pages 312–321. ACM, 2003.

[CT95] Timothy F Cootes and Christopher J Taylor. Combining point distribution models with shape models based on finite element analysis. *Image and Vision Computing*, 13(5):403–409, 1995.

[CTCG95] Timothy F Cootes, Christopher J Taylor, David H Cooper, and Jim Graham. Active shape models-their training and application. *Computer vision and image understanding*, 61(1):38–59, 1995.

[CUC07] James C Coburn, Mohammad A Upal, and Joseph J Crisco. Coordinate systems for the carpal bones of the wrist. *Journal of biomechanics*, 40(1):203–209, 2007.

[DCLCC05] Ugo Della Croce, Alberto Leardini, Lorenzo Chiari, and Aurelio Cappozzo. Human movement analysis using stereophotogrammetry: Part 4: assessment of anatomical landmark misplacement and its effects on joint kinematics. *Gait & posture*, 21(2):226–237, 2005.

[DCT01] Rhodri H Davies, Tim F Cootes, and Chris J Taylor. A minimum description length approach to statistical shape modelling. In *Biennial International Conference on Information Processing in Medical Imaging*, pages 50–63. Springer, 2001.

[DDK+17] Priscilla D'agostino, Benjamin Dourthe, Faes Kerkhof, Filip Stockmans, and Evie E Vereecke. In vivo kinematics of the thumb during flexion and adduction motion: Evidence for a screw-home mechanism. *Journal of Orthopaedic Research*, 35(7):1556–1564, 2017.

[DTS03] Christos Davatzikos, Xiaodong Tao, and Dinggang Shen. Hierarchical active shape models, using the wavelet transform. *IEEE transactions on medical imaging*, 22(3):414–423, 2003.

[DTT08] Rhodri Davies, Carole Twining, and Chris Taylor. *Statistical models of shape: Optimisation and evaluation*. Springer Science & Business Media, 2008.

[Duv14] David Duvenaud. *Automatic model construction with Gaussian processes*. PhD thesis, University of Cambridge, 2014.

[GM98] Ulf Grenander and Michael I Miller. Computational anatomy: An emerging discipline. *Quarterly of applied mathematics*, 56(4):617–694, 1998.

[HBM+92] Anne Hollister, William L Buford, Loyd M Myers, David J Giurintano, and Andrew Novick. The axes of rotation of the thumb carpometacarpal joint. *Journal of Orthopaedic Research*, 10(3):454–460, 1992.

[HM09] Tobias Heimann and Hans-Peter Meinzer. Statistical shape models for 3d medical image segmentation: a review. *Medical image analysis*, 13(4):543–563, 2009.

[HRG+13] Eni Halilaj, Michael J Rainbow, Christopher J Got, Douglas C Moore, and Joseph J Crisco. A thumb carpometacarpal joint coordinate system based on articular surface geometry. *Journal of biomechanics*, 46(5):1031–1034, 2013.

[HRG+14] Eni Halilaj, Michael J Rainbow, Christopher Got, Joel B Schwartz, Douglas C Moore, Arnold-Peter C Weiss, Amy L Ladd, and Joseph J Crisco. In vivo kinematics of the thumb carpometacarpal joint during three isometric functional tasks. *Clinical Orthopaedics and Related Research®*, 472(4):1114–1122, 2014.

[JL06] Lynette A Jones and Susan J Lederman. *Human hand function*. Oxford University Press, 2006.

[Jol11] Ian Jolliffe. *Principal component analysis*. Springer, 2011.

[KOT+18] Yohei Kawanishi, Kunihiro Oka, Hiroyuki Tanaka, Kiyoshi Okada, Kazuomi Sugamoto, and Tsuyoshi Murase. In vivo 3-dimensional kinematics of thumb carpometacarpal joint during thumb opposition. *The Journal of hand surgery*, 43(2):182–e1, 2018.

[KWT88] Michael Kass, Andrew Witkin, and Demetri Terzopoulos. Snakes: Active contour models. *International Journal of Computer Vision*, 1(4):321–331, Jan 1988.

[Lé] Bruno Lévy. Graphite.

[LFGV17] Marcel Lüthi, Andreas Forster, Thomas Gerig, and Thomas Vetter. Shape modeling using gaussian process morphable models. In *Statistical Shape and Deformation Analysis*, pages 165–191. Elsevier, 2017.

[LGJV17] Marcel Lüthi, Thomas Gerig, Christoph Jud, and Thomas Vetter. Gaussian process morphable models. *IEEE transactions on pattern analysis and machine intelligence*, 40(8):1860–1873, 2017.

[LJV13] Marcel Lüthi, Christoph Jud, and Thomas Vetter. A unified approach to shape model fitting and non-rigid registration. In *International workshop on machine learning in medical imaging*, pages 66–73. Springer, 2013.

[MCTL07] Douglas C Moore, Joseph J Crisco, Theodore G Trafton, and Evan L Leventhal. A digital database of wrist bone anatomy and carpal kinematics. *Journal of biomechanics*, 40(11):2537–2542, 2007.

[MvdWN+10] Michelle Marshall, Danielle van der Windt, Elaine Nicholls, Helen Myers, and Krysia Dziedzic. Radiographic thumb osteoarthritis: frequency, patterns and associations with pain and clinical assessment findings in a community-dwelling population. *Rheumatology*, 50(4):735–739, 2010.

[NHBT07] Delphine Nain, Steven Haker, Aaron Bobick, and Allen Tannenbaum. Multiscale 3-d shape representation and segmentation using spherical wavelets. *IEEE Transactions on Medical Imaging*, 26(4):598–618, 2007.

[WC95] Ge Wu and Peter R Cavanagh. Isb recommendations for standardization in the reporting of kinematic data. *Journal of biomechanics*, 28(10):1257–1261, 1995.

[WS00] Yongmei Wang and Lawrence H Staib. Boundary finding with prior shape and smoothness models. *IEEE Transactions on Pattern Analysis and Machine Intelligence*, 22(7):738–743, 2000.

[WS01] Christopher KI Williams and Matthias Seeger. Using the nyström method to speed up kernel machines. In *Advances in neural information processing systems*, pages 682–688, 2001.

[WVdHV+05] Ge Wu, Frans CT Van der Helm, HEJ DirkJan Veeger, Mohsen Makhsous, Peter Van Roy, Carolyn Anglin, Jochem Nagels, Andrew R Karduna, Kevin McQuade, Xuguang Wang, et al. Isb recommendation on definitions of joint coordinate systems of various joints for the reporting of human joint motion—part ii: shoulder, elbow, wrist and hand. *Journal of biomechanics*, 38(5):981–992, 2005.

[ZAT05] Zheen Zhao, Stephen R. Aylward, and Eam Khwang Teoh. A novel 3d partitioned active shape model for segmentation of brain mr images. In James S. Duncan and Guido Gerig, editors, *Medical Image Computing and Computer-Assisted Intervention – MICCAI 2005*, pages 221–228, Berlin, Heidelberg, 2005. Springer Berlin Heidelberg.